Front matter

Full title

Functional alterations of salience-related networks are associated with traits, staging, and the state of psychosis

Short title

Salience-related network alteration in psychosis

Authors

Jun Miyata[1,4]*, Toby Winton-Brown[4], Thomas Sedlak[5], Toshihiko Aso[8], Nicola Cascella[5], Jennifer Coughlin[5], Nicolas A. Crossley[4,19], Emrah Duezel[31], Takahiro Ezaki[26], Masaki Fukunaga[17], Carolyn Howell[5], Masanori Isobe[1], Kouhei Kamiya[29], Kiyoto Kasai[25,28], Takanori Kochiyama[10], Shinsuke Koike[23,24,27,28], Akira Kunimatsu[12], Naoki Masuda[21,22], Susumu Mori[6], Yasuo Mori[1], Toshiya Murai[1], Kiyotaka Nemoto[34], Frederick Nucifora[5], Kazutaka Ohi[11,14], Naohiro Okada[25,28], Yuki Sakai[9], Nobukatsu Sawamoto[2], Tsutomu Takahashi[32,33], Shinichi Urayama[3], Yoshiyuki Watanabe[20], Crystal C. Watkins[5], Hidenaga Yamamori[13,16,18], Yuka Yasuda[15,16], Ryota Hashimoto[16], Hidehiko Takahashi[1,30], Akira Sawa[5,7], Philip McGuire[4]

Affiliations

[1] Department of Psychiatry, Graduate School of Medicine, [2] Department of Human Health Sciences, Graduate School of Medicine, [3] Human Brain Research Center, Graduate School of Medicine, Kyoto University, Kyoto, Japan

[4] Department of Psychosis Studies, Institute of Psychiatry, Psychology & Neuroscience,

King's College London, London, United Kingdom

[5] Departments of Psychiatry, Neuroscience, Biomedical Engineering and Genetic Medicine, School of Medicine, [6] Department of Radiology, School of Medicine, [7] Department of Mental Health, Bloomberg School of Public Health, Johns Hopkins University, Baltimore, MD, United States

[8] Laboratory for Brain Connectomics Imaging, RIKEN Center for Biosystems Dynamics Research, Kobe, Japan

[9] Brain Information Communication Research Laboratory Group, Advanced Telecommunications Research Institutes International, Kyoto, Japan

[10] Brain Activity Imaging Center, ATR-Promotions, Kyoto, Japan

[11] Department of Psychiatry, Gifu University Graduate School of Medicine, Gifu, Japan

[12] Department of Radiology, International University of Health and Welfare Mita Hospital, Tokyo, Japan

[13] Japan Community Health care Organization Osaka Hospital, Osaka, Japan

[14] Department of General Internal Medicine, Kanazawa Medical University, Uchinada, Ishikawa, Japan

[15] Medical Corporation Foster, Osaka, Japan

[16] Department of Pathology of Mental Diseases, National Institute of Mental Health, National Center of Neurology and Psychiatry, Kodaira, Tokyo, Japan

[17] Department of System Neuroscience, Division of Cerebral Integration, National Institute for Physiological Sciences, Okazaki, Japan

[18] Department of Psychiatry, Osaka University Graduate School of Medicine, Suita, Osaka, Japan

[19] Department of Psychiatry, Pontificia Universidad Catolica de Chile, Santiago, Chile

[20] Department of Radiology, Shiga University of Medical Science, Shiga, Japan

[21] Department of Mathematics, [22] Computational and Data-Enabled Science and Engineering Program, State University of New York at Buffalo, Buffalo, NY, United States

[23] Center for Evolutionary Cognitive Sciences (ECS), Graduate School of Art and Sciences, [24] Center for Integrative Science of Human Behavior (CiSHuB), [25] Department of Neuropsychiatry, Graduate School of Medicine, [26] Division of Advanced Logistic Science, Research Center for Advanced Science and Technology, [27] Institute for Diversity & Adaptation of Human Mind (UTIDAHM), [28] International Research Center for Neurointelligence (WPI-IRCN), Institute for Advanced Study (UTIAS), The University of Tokyo, Tokyo, Japan

[29] Department of Radiology, Toho University Omori Medical Center, Tokyo, Japan

[30] Department of Psychiatry and Behavioral Sciences, Graduate School of Medical and Dental Sciences, Tokyo Medical and Dental University, Tokyo, Japan

[31] Institute of Cognitive Neuroscience, University College London, London, United Kingdom

[32] Department of Neuropsychiatry, Graduate School of Medicine and Pharmaceutical Sciences, [33] Research Center for Idling Brain Science, University of Toyama, Toyama, Japan

[34] Department of Psychiatry, Faculty of Medicine, University of Tsukuba, Ibaraki, Japan

*** Corresponding author**

Jun Miyata, MD, PhD

Department of Psychiatry, Graduate School of Medicine, Kyoto University

54 Shogoin-Kawaharacho, Sakyo-ku, Kyoto 606-8507, Japan

Tel: +81-75-751-3386

Fax: +81-75-751-3246

E-mail: miyata10@kuhp.kyoto-u.ac.jp

Abstract

Aberrant salience is essentially implicated in psychosis, involving the midbrain-striatum-hippocampus and anterior cingulate cortex-insula (salience network: SN) systems. However, how these two systems contribute to psychosis traits, staging, and state remains unclear. Thus, we conducted an international multi-site resting functional magnetic resonance imaging study of 209 ultra-high-risk (UHR), first-episode (FEP), and chronic (ChrP) psychosis patients and 279 healthy controls. After intensive denoising and site effect-harmonization, we found 1) reduced connectivity and increased instability of two salience-related systems in the UHR and FEP, in which the SN's significance levels/effect sizes were in the order of UHR > FEP > ChrP 2) an association between stronger connectivity of the midbrain-striatum-hippocampus system and severer delusions and hallucinations in FEP 3) attenuation of finding 2 in patients with medication and non-affective psychosis. The results suggest that the two salience-related systems are associated with psychosis traits, staging, and state in different ways.

Teaser

Two salience-related functional networks are associated with psychosis traits, staging, and state, in different ways.

Main text

Introduction

The term salience denotes the quality of being particularly noticeable or important (Oxford Dictionary https://www.lexico.com) and is computationally defined as the absolute value of the prediction error (1) and Laplacian (2) of stimuli. For survival, animals must quickly allocate their limited attentional resources to salient stimuli in the surrounding world. Previous animal studies have shown that midbrain-striatal dopaminergic activity codes motivational (reward and avoidance) salience (3–5), while human functional magnetic resonance imaging (fMRI) studies have revealed that the striatum is responsive to stimulus salience (6–9).

Alterations in the midbrain and striatum are indicated in psychosis (10). Psychosis is a broad term for severe mental disorders with delusions and/or hallucinations (i.e., positive symptoms (11)), the most common of which is schizophrenia. Elevated dopamine levels in the striatum of patients with schizophrenia (12) have been hypothesized to cause aberrantly heightened salience attribution to ordinary stimuli, leading to delusions and hallucinations (aberrant salience hypothesis) (10). Additionally, recent circuit models of psychosis indicate that overactivity of glutamatergic neurons in the hippocampus triggers midbrain activation, leading to a hyperdopaminergic state in the striatum (13). These findings are consistent with those of recent studies in patients with psychosis (14, 15). Thus, the midbrain-striatum-hippocampus system plays a critical role in aberrant salience in psychosis.

Human fMRI studies have described another neural system, the “salience network (SN),” which mainly comprises the anterior cingulate cortex (ACC) and bilateral insula, and it is activated by the salience of stimuli rather than the nature of tasks (16, 17). Studies have reported SN alterations in schizophrenia patients (18–20). However, a critical unanswered question is the role of the ACC-insular SN system in the aberrant salience of psychosis.

Alternatively, how do these two salience-related systems contribute to the pathophysiology of psychosis?

Resting-state fMRI (rsfMRI), fMRI scanning while at rest, is widely used to investigate the functional connectivity of brain networks in psychiatric disorders. Independent component analysis (ICA) is a common method used to analyze functional connectivity in rsfMRI. ICA can identify intrinsic functional networks representing the midbrain-striatum-hippocampus system and the ACC-insular SN system in a data-driven manner; the midbrain and striatum were identified as the basal ganglia network (BGN (21)): the bilateral hippocampus was identified within the medial temporal lobe network (MTLN (22), also known as the meso/paralimbic network (23)), and the SN comprised the ACC and insula (16). Investigating the connectivity within and between these three networks could answer the questions raised above.

The development of objective biomarkers is necessary for the diagnosis, prevention, and treatment of psychosis. Biomarkers are generally categorized as 1) trait markers, which are present throughout the disease course and are not changed by treatment; 2) staging markers, which are prominent in certain disease stages; and 3) state markers, which reflect symptoms and changes according to the treatment (24–27). The course of psychosis can be divided into ultra-high-risk (UHR), post-onset or first-episode psychosis (FEP), and chronic psychosis (ChrP) stages (28). It is unclear whether aberrant salience is associated with psychosis traits, stage, or state.

Thus, we aimed to investigate how the two salience-related systems are associated with the aberrant salience of psychosis using ICA of rsfMRI. Our main outcomes were whether functional connectivity within and between the BGN, MTLN, and SN was associated with the 1) diagnosis of psychosis and/or 2) positive symptom severity at the UHR, FEP, and ChrP stages. The secondary outcomes were whether antipsychotic medication and psychosis type (affective or non-affective) affected the findings of 1) and 2), and clarifying the meaning

of the findings. To fully describe the connectivity profile, we investigated dynamic (29) (temporally varying) network measures, as well as static (temporally constant) (30) measures. Considering that antipsychotics (dopamine blockers) work on psychotic symptoms, we hypothesized that the midbrain-striatum-hippocampus system would be associated with positive symptoms as well as medication.

Results

Participant characteristics

We recruited 1) 29 individuals with UHR and 25 age-, sex-, and ethnicity-matched healthy controls (HC); 2) 81 patients with FEP and 109 matched HC; and 3) 99 patients with ChrP and 145 matched HC, comprising 488 subjects in total, from eight scanners (sites) at seven institutes. Each site/institute is listed in Table 1 and in the Methods section, and detailed participant characteristics at each institute are described in the Supplemental Methods and Supplemental Tables 1-7 in the Supplemental Material. Here, we refer to the individuals with UHR as patients (PT), as well as FEP and ChrP for convenience.

Positive symptom severity and overall psychopathology were indexed by the Comprehensive Assessment of At-Risk Mental States (CAARMS) (31) for UHR, and the Positive and Negative Syndrome Scale (PANSS) (32) for FEP and ChrP.

The number of years of completed education was lower in PT than in HC at all stages, and smoking and substance use were more prevalent in the FEP group than in the HC group (Table 1).

Summary of data analysis pipeline

The rsfMRI and structural MRI data were acquired using 3-Tesla MRI at each site. Details of

the MRI acquisition parameters at each site are provided in Supplemental Table 8. After preprocessing of the rsfMRI data, including denoising by independent component analysis (ICA) (33) (see Methods), we identified group-level networks of interest (NOIs: BGN, MTLN, and SN) by performing meta-ICA (see Methods) (34, 35). Next, we performed thresholded dual-regression (TDR) (36) to calculate the subject-specific spatial maps and time courses of each component. We then analyzed the dynamics of the NOIs' time courses using energy landscape analysis (ELA) (37–42) (see Methods). Before the statistical analysis, we removed the site effect by harmonization using ComBat (43–45) (see Methods). Finally, we performed group comparisons and correlation analyses with psychotic symptom severity for 1) within-network connectivity using spatial maps, 2) between-network connectivity using the Z-transformed partial correlation coefficients between time courses of each NOI-pair controlling for other NOIs, and 3) dynamics of the time courses. Full multiple-comparison correction was performed (see Methods section). The effects of age, sex, and temporal signal-to-noise ratio (tSNR) of the rsfMRI data were controlled.

Group-level networks of interest and their dynamics

Meta-ICA identified the NOIs as shown in Figure 1. The BGN was split into the subnetworks of the midbrain-thalamus part (BGN-MbThal) and striatum part (BGN-Str), and the SN was split into the ACC part (SN-ACC) and insula part (SN-Ins). Thus, we had five NOIs in total. Hierarchical clustering based on the time course of each NOI revealed that these subnetworks were close to each other (Figure 1).

Next, we investigated the dynamic relationship between NOIs by applying ELA to the NOI time courses (see Methods). Based on whether the time course was above or below the mean, we classified the activity patterns of the five NOIs into 2^5 = 32 patterns, which were aggregated into two brain states (Figure 2a). State A had local minima (frequent, low-energy

pattern) with all five NOIs "deactivated" (below the mean of the time series, Black in Figure 2b), whereas all NOIs were "activated" in state B (above the mean of the time series, White in Figure 2b). Figure 2c shows that these two states have low energies (stable).

Within-network connectivity was reduced, and brain state transition was increased in early psychosis stages

As the first main outcome, we performed group comparisons of the network measures at each psychosis stage. For within-network connectivity, we compared spatial maps derived using TDR. At the UHR stage, we found that connectivity within the SN-ACC was significantly reduced in the ACC in PT compared to matched HC ($p = 0.003$, corrected for the number of voxels by threshold-free cluster enhancement (46), two contrasts, and five networks) (Figure 3a, left). At the FEP stage, we also found significantly reduced connectivity within the BGN-MbThal in the right thalamus in the PT group compared to that in the HC group ($p = 0.02$, corrected for voxel, contrast, and network) (Figure 3a, right).

Notably, at more liberal thresholds, the SN-ACC also showed reduced connectivity in FEP ($p = 0.07$, corrected for voxels, contrast, and network) and ChrP ($p = 0.08$, corrected for voxels and contrast) at almost the same locations as in UHR (Figure 3b). The effect sizes (Hedges' g) of these significant clusters for UHR, FEP, and ChrP were 1.45, 0.60, and 0.54, respectively (Figure 3c). Other significant results at liberal thresholds are shown in Supplementary Figure 1.

We then performed group comparisons of between-network connectivity at each stage using the Z-transformed partial correlation coefficients between pairs of NOI time courses derived by TDR. We found no significant difference in the correlation coefficients between PT and matched HC at any stage, even at liberal thresholds.

We performed group comparisons of two ELA indices: the frequency of state B (note that the frequency of state A can be calculated as 1 – state B) and the transition rate between states A and B. We found a significant increase in the transition rate between states A and B for FEP compared to that of matched HC ($p = 0.003$, corrected for two contrasts and two indices) (Figure 3d). No other significant differences were observed even at liberal thresholds.

Within- and between-network connectivity of the MTLN was positively correlated with positive symptom severity in FEP

As the second main outcome, we performed correlational analyses between connectivity measures and positive symptom severity at each stage. For the within-network connectivity, we found a significant positive correlation between the PANSS positive score and the MTLN in the left/right hippocampus and parahippocampal gyrus in the FEP group ($p = 0.03$ and $p = 0.02$ for the left and right, respectively, corrected for voxel, contrast, and network) (Figure 4a). Figure 4b shows the scatter plot of the mean cluster values. Figure 4c shows the same scatter plot colored by site, indicating that there was no clear site effect for this result. Supplementary Figure 2a also shows the results at liberal thresholds. No other significant correlations were found.

We then investigated the correlation between between-network connectivity and severity of positive symptoms. We found a significant positive correlation between the PANSS positive score and the connectivity between the MTLN and BGN-MbThal in FEP ($p = 0.04$, corrected for contrast and network) (scatter plot in Figure 4d). Figure 4e shows the plot by site and indicates no clear site effects. Supplementary Figure 2b also shows

significant results at liberal thresholds in UHR and FEP. No other significant correlations were found.

The ELA indices did not show significant correlations with positive symptoms even at liberal thresholds.

Positive correlation between connectivity and positive symptoms was stronger in unmedicated than in medicated patients

As the secondary outcome, we then investigated the effect of antipsychotic medication on the significant results above. In the group comparison results, only one UHR individual was administered a low dose of quetiapine (50 mg). Thus, we removed this subject and performed group comparison of the cluster value of the ACC of the SN-ACC, and the group difference remained significant ($p < 0.001$, corrected for contrast). For FEP, the Johns Hopkins University (JHU) site had both unmedicated ($n = 4$) and medicated ($n = 47$) patients. Thus, we compared the cluster value of the right thalamus of the BGN-MbThal, and there was no significant difference between the unmedicated and medicated patients ($p = 0.63$, corrected for contrast). This was replicated when all six sites were used ($p = 0.67$, corrected for contrast). We also investigated the ELA result similarly and found no significant difference between unmedicated and medicated patients ($p = 0.48$ and 0.12 for JHU and all six sites, respectively, corrected for contrast). In summary, we did not find a significant effect of antipsychotic medication on group comparison results.

For the significant correlation analysis results for FEP, we investigated whether there was an interaction between medication and PANSS positive scores on the connectivity values. For the within-network connectivity results, we found significant interactions between

medication and PANSS on the mean cluster value of the MTLN, both for the JHU site ($p < 0.001$, corrected for contrast. Figure 5a, left) and for all six sites ($p = 0.009$, corrected for contrast). Figure 5a right). This indicated a steeper regression slope in unmedicated patients than in medicated patients. For the between-network connectivity results, we also found significant interactions between medication and PANSS on the connectivity between the MTLN and BGN-MbThal, for the JHU site ($p < 0.001$, corrected for contrast. Figure 5b, left) as well as all six sites ($p = 0.01$, corrected for contrast). Figure 5b right). These results also indicated a steeper regression slope in unmedicated patients than that in medicated patients. In summary, the positive correlation between the within- and between-network connectivity of the MTLN and positive symptoms was stronger in unmedicated than in medicated FEP patients.

Positive correlation between connectivity and positive symptoms was stronger in affective than in non-affective psychosis patients

As the other secondary outcome, we investigated whether the significant results above in FEP were different between affective psychosis (major depressive disorder or bipolar disorder with psychotic symptoms) and non-affective psychosis (schizophrenia spectrum) patients. For the group comparison results, the JHU site had both affective ($n = 14$) and non-affective ($n = 37$) psychosis patients, and we compared the cluster value of the thalamus of the BGN-MbThal between them. We found no group difference ($p = 0.84$, corrected for contrast), which was consistent when we included all six sites ($p = 0.37$, corrected for contrast). The transition rate between the two brain states did not differ between psychosis types for the JHU site and all six sites ($p = 0.27$ and 0.13 for the JHU and all six sites, respectively,

corrected for contrast). In summary, we did not find a significant effect of psychosis type on group differences.

For the significant correlation analysis results in the FEP stage, we investigated whether there was an interaction between psychosis type and PANSS positive scores on connectivity values. For the within-network connectivity result, we found significant interactions between psychosis type and PANSS on the mean cluster value of the MTLN, both for the JHU site ($p < 0.001$, corrected for contrast. Figure 6a, left) and for all six sites ($p = 0.003$, corrected for contrast). Figure 6a right). This indicated a steeper regression slope in affective than in non-affective psychosis patients. For the between-network connectivity result, we also found significant interactions between psychosis type and PANSS on the connectivity between the MTLN and BGN-MbThal, both for the JHU site ($p < 0.001$, corrected for contrast. Figure 6b, left) and all six sites ($p = 0.001$, corrected for contrast). Figure 6b right). These results also indicated a steeper regression slope in affective than in non-affective psychosis patients. In summary, the positive correlations between within- and between-network connectivity of the MTLN and positive symptoms were stronger in patients with affective FEP than in those with non-affective FEP.

Comorbidity did not affect group differences, while it weakened the correlation between connectivity and positive symptoms

Ten UHR individuals from the Institute of Psychiatry, Psychology, and Neuroscience (IoPPN) site and six FEP patients from the JHU site had comorbid psychiatric disorders besides schizophrenia spectrum or mood disorders, as described in Supplementary Methods. To supplementarily investigate whether our results are associated with psychosis per se or rather general psychopathology common to psychiatric disorders (47), we divided the patients into

those with or without comorbidity at these sites. There was no effect of comorbidity on any of the significant group difference results as detailed in Supplementary Results.

For the significant correlation of the within-network connectivity of FEP, the cluster value of the hippocampus of the MTLN showed a trend-level interaction between comorbidity and the PANSS positive score ($p = 0.08$, corrected for contrast. (Supplemental Figure 3). For the significant correlation of the between-network connectivity of FEP, there was a significant interaction between comorbidity and PANSS positive score on the connectivity between MTLN and BGN-MbThal ($p = 0.03$, corrected for contrast, Figure 7). Sub-analysis showed a trend-level positive correlation in patients without comorbidity ($p = 0.06$, corrected for contrast), whereas no correlation was found in patients with comorbidity ($p = 0.279$). In summary, these results indicate that our correlational findings were specific to psychosis rather than to the general psychopathology common to psychiatric disorders.

Smoking did not affect group differences, while it may weaken correlation between connectivity and positive symptoms

We further investigated the possible confounding effects of smoking on the results. There was no effect of smoking on the group difference results (details in the Supplementary Results).

For the significant correlation of the within-network connectivity of FEP, the cluster value of the hippocampus of the MTLN showed a trend-level interaction between smoking and the PANSS positive score ($p = 0.07$, corrected for contrast. Supplemental Figure 4a). For the significant correlation of the between-network connectivity of FEP, there was also a trend-level interaction between smoking and PANSS positive score on the connectivity between the MTLN and BGN-MbThal ($p = 0.052$, corrected for contrast. Supplemental Figure 4b). In summary, smoking might undermine the correlation between connectivity and

positive symptoms.

Substance use did not affect group difference or correlational results

Since four UHR individuals from the IoPPN site and 11 FEP patients from the JHU site had experience with substance use, we investigated its effect on the above results at these sites. The details are provided in Supplementary Results. In summary, there were no effects of substance use on group differences or correlations with PANSS positive symptoms, even at a liberal threshold ($p < 0.05$, uncorrected).

Discussion

The main findings of this study are the following:

1: Reduced within-network connectivity and increased instability of the two salience-related systems were observed in UHR and FEP, with the SN showing significance levels and effect sizes in the order of UHR > FEP > ChrP.

2: Stronger connectivity within and between the midbrain-striatum-hippocampus system was associated with severer positive symptoms in FEP.

3: Finding 1 was not affected by medication or psychosis type, while finding 2 was attenuated in medicated and non-affective psychosis patients.

Collectively, we found fully corrected significance in UHR and FEP but not in ChrP, indicating that aberrant salience is more “salient” at early stages of psychosis (48). These findings are discussed in the following sections.

Salience-related functional measures represent trait/staging of psychosis

Regarding the midbrain-striatum-hippocampus system, we found reduced connectivity in the thalamus of the BGN in patients with FEP. We recently reported heightened resting

connectivity between the thalamus and cortical areas in patients with FEP (49) in a sample that partially overlapped with the present study. Moreover, the thalamus has also recently been reported to process salience (50).The current results have thus extended our knowledge of the underlying structure of aberrant salience in psychosis. In contrast, we did not observe altered within-network connectivity in the striatum of the BGN, while two previous ICA studies reported increased within-network connectivity (51, 52). Compared with these studies, we thoroughly considered confounding factors, as detailed in the Methods section, and strongly controlled these for multiple comparisons.

For the ACC-insular SN system, we found reduced within-network connectivity, with significance levels and effect sizes in the order of UHR > FEP > ChrP, in almost the same locations in the ACC (Figure 3b). This finding indicates that SN alterations may be present throughout the stages and may weaken in later stages. These findings are also largely consistent with those of previous ICA studies reporting reductions in within-network connectivity of the SN in patients with schizophrenia (53–57).

This is the first ELA study to reveal frequent transitions between two brain states, that is, increased instability of salience-related networks in FEP. Several previous studies have reported increased instability among the SN, frontoparietal network (FPN), and default mode network (DMN) in schizophrenia, consistent with our findings (58, 59). The finding of synchronized fluctuations of all five NOIs in the two brain states is consistent with our view that the integration of different salience systems plays a key role in the pathophysiology of psychosis (60).

Importantly, these findings were not affected by medication, psychosis type, comorbidity, smoking, or substance use. Therefore, the within-network connectivity and brain-state transition of the two salience-related systems are candidates for early-stage markers of psychosis; moreover, the ACC-insular SN system may also serve as a trait marker.

Midbrain-striatum-hippocampus functional connectivity represents psychosis state

We observed an association between severer positive symptoms and stronger functional connectivity within the MTLN and between the MTLN and BGN-MbThal in patients with FEP. No other study has investigated the MTLN in psychosis using rsfMRI and ICA; thus, this finding is not only new but also important, as the hippocampus is postulated to be the starting point of dopaminergic aberrant salience in psychosis (13). The midbrain region of BGN-MbThal was also correlated with positive symptoms, although at a liberal threshold (Supplementary Figure 2a).

Importantly, these associations were attenuated in the medicated patients, consistent with the requirement for state markers of psychosis (25, 26). We also found that this association was stronger in patients with affective psychosis than those with non-affective psychosis. Since affective psychosis has better treatment responsiveness than non-affective psychosis (61), these findings may represent responsiveness to antipsychotic medications. The finding that these associations were weakened by comorbidity and might be weakened by smoking is not contradictory to this state-marker view.

We did not observe an association between positive symptoms and connectivity of the ACC-insular SN system at a fully corrected level, although we did observe an association at liberal thresholds (Supplementary Figure 2b). Taken together, these findings suggest that the functional connectivity of the midbrain-striatum-hippocampus system is a candidate for state marker of aberrant salience, more so than the ACC-insular SN system.

Relationship with other networks

Salience plays a key role in attention allocation, and the association between salience systems, especially the SN and attentional system, such as the dorsal attention network, is important (62, 63). In addition, SN is the network included in the "triple network model," which postulates that the SN acts as a switch between the DMN that is activated during rest,

and the FPN that is activated on task (64, 65). While admitting their importance, in this study we focused on the networks related to salience per se, hypothesizing that they were directly related to the pathophysiology of aberrant salience in psychosis.

Robustness of the findings

The strengths of this study include the large sample size, intensive data denoising, robust estimation of intrinsic networks by meta-ICA, accurate estimation of the network time course by TDR, site-effect harmonization using ComBat, and intensive multiple comparison correction.

A patient with the highest connectivity value in the correlational analyses may appear to be an outlier, although Cook's distance (<0.5) indicated that this was not the case. We supplementarily excluded this subject, and the main outcome of the correlation with positive symptoms remained significant. The secondary outcomes of the effect of medication on the correlational analysis turned into trend level, and the effects of psychosis type disappeared (Supplementary Results). These findings might indicate that the findings of medication were more robust than those of psychosis type.

Limitations

First, owing to the relative difficulties in recruiting UHR individuals and organizing a multi-site study, the UHR sample size was small compared to that of FEP and ChrP. Second, medication and psychosis types were not perfectly balanced among the sites, as shown in Table 1 and as described in the Methods section. However, our results indicate that harmonization has effectively managed this problem. Third, susceptibility-induced distortion correction was not performed since several sites did not have the field map necessary for this procedure. Fourth, the longitudinal study design would be more suitable. However, to cover

all stages, at least10 years of follow-up is required, making such a design unrealistic. Finally, to develop clinically usable biomarkers, our findings require translation into more standardizable frameworks, such as multi-feature-based parcellation (66) and/or combination with other modalities (49, 67–69).

Conclusions

Functional alterations of the two salience-related systems, the midbrain-striatum-hippocampus system and ACC-insular SN systems, were mainly associated with the early stages of psychosis. Alteration of the latter was associated with the staging and possibly traits of psychosis, while the former was associated with the psychosis state, reflecting both positive symptoms and antipsychotic treatment. Further refinement of these findings is necessary for precision psychiatry. Our focus on certain pathophysiological models/hypotheses (aberrant salience), identification of networks in a data-driven manner, and utilization of state-of-the-art denoising and harmonization methods will benefit research on a wide range of psychiatric disorders.

Methods

Details of participants and sites

We recruited the UHR, FEP, and ChrP subjects as well as the matched HC individuals at the following eight scanners (sites) from seven institutes: the Institute of Psychiatry, Psychology, and Neuroscience (IoPPN), UK; Johns Hopkins University Hospital (JHU), USA; Kanazawa Medical University (KMU), Japan; Kyoto University (Kyoto), Japan; two MRI scanners of Osaka University (OSK), Japan; the University of Tokyo (Tokyo), Japan; and the University of Toyama (TYM), Japan (Table 1). The details of participant characteristics of each institute are described in Supplemental Methods and Supplemental Tables 1-7. The Japanese sites

were members of the Cognitive Genetic Collaborative Research Organization (COCORO) consortium.

UHR was defined according to CAARMS (31). FEP and ChrP were defined as duration of illness (DOI) of ≤ 36 months and > 36 months, respectively. UHR individuals from IoPPN were unmedicated with antipsychotics, except for one patient (50 mg quetiapine). The JHU had both unmedicated (n = 4) and medicated (n = 47) FEP patients. All FEP and ChrP patients from the KMU, OSK, and TYM groups were unmedicated while all patients with FEP and ChrP from Kyoto and Tokyo were medicated in this study. JHU had both affective (N=14, major depressive disorder or bipolar disorder with delusions/hallucinations) and non-affective (N=37, schizophrenia spectrum) psychosis patients. All Japanese sites had non-affective psychosis patients only.

Symptomatology was assessed using CAARMS for UHR as described above. For FEP and ChrP, 1) combination of the Scale for the Assessment of Positive Symptoms (SAPS) (70) and the Scale for the Assessment of Negative Symptoms (SANS) (71), or 2) PANSS (32) were used at each site. The SAPS global summary score was converted to the PANSS positive score (72).

After receiving a complete description of the study, all the participants provided written informed consent. The study design was approved by the institutional review board of each institution:

approved by Hammersmith Hospital Research Ethics Committee (IoPPN);

approved by Johns Hopkins Medicine Institutional Review Board (JHM IRB) (JHU);

approved by Research Ethical Committee of Kanazawa Medical University (KMU);

approved by Kyoto University Graduate School and Faculty of Medicine, Ethics Committee (Kyoto);

approval by Research Ethics Committee, Osaka University (OSK);

approved by Research Ethics Committee of the Faculty of Medicine of the University of Tokyo (Tokyo);

and approved by Ethics Committee, University of Toyama (TYM).

MRI acquisition

The details of the scanning parameters are provided in Supplemental Table 8. All MRI images were visually checked, and subjects with gross artifacts or anatomical anomalies were excluded from this study. Subjects with excessive head motion (mean framewise displacement (73) of > 0.5 mm) were also not enrolled in this study.

Preprocessing of the MRI data including ICA-based denoising

Head-motion correction was performed using SPM8 (Wellcome Department of Cognitive Neurology, London, United Kingdom) running on Matlab (MathWorks), followed by spatial normalization to the MNI template brain using the T1 anatomical image.

ICA-based denoising was performed for each participant to remove non-neuronal signals (head motion, physiological noise such as pulsation and respiration, and machine-derived noise) from the fMRI data (for the details please refer to Aso et al, 2017 (33)). Functional images were fed into MELODIC/FSL (http://www.fmrib.ox.ac.uk/fsl) with automatic component number estimation. Instead of picking up several subjects as a training sample for machine-learning and classifying the components of other subjects into neuronal and noise components (74, 75), we classified all subjects' components based on three objective criteria: 1) high-frequency power ratio (>0.1 Hz up to 0.2 Hz or the Nyquist frequency for the TR) relative to <0.1 Hz, 2) non-gray matter involvement index, and 3) slice dependency index calculated as the ratio of within- and between-slice spatial high-frequency components. The thresholds at each site are shown in Supplemental Table 9. Figure 8 shows

the components with the top 12 variances for an example subject. Components with high high-frequency power ratio (HF), high slice dependency index (SL), or high non-gray matter index (NB) were classified as noise (surrounded by yellow frame), while components with neuronal origin were preserved (surrounded by blue). Each component was interpreted according to a previous machine-learning-based protocol (74, 75), showing consistency with our objective criteria. The all 62 components of this subject are shown in Supplemental Figure 5. The effect of our ICA-based denoising is also shown in Supplemental Video 1, which contrasts the non-denoised (left) and denoised (right) rsfMRI data.

After ICA denoising, the rsfMRI data were normalized into the MNI 152 space using the unified segmentation algorithm of SPM8. Data were then re-sampled into 3 mm isotropic voxel and smoothed by a Gaussian kernel of full width at half maximum of 5 mm. Since the minimum number of volumes was 150 (Supplemental Table 8), we used 145 volumes for each site and discarded the first five volumes for signal stabilization.

As an index of data quality, the tSNR was calculated at each voxel as the mean/SD of the time course and it was averaged for the whole brain using QAscript **(**76**).**

Meta-ICA

ICA utilizes a probabilistic algorithm for component estimation, and it includes the problem of reproducibility. Therefore, we performed meta-ICA (34, 35), which has higher robustness and reproducibility than conventional single-shot group ICA (gICA) (77). The meta-ICA in this study comprised of two steps:

First step: Preprocessed data of five PT and five HC were randomly selected from each site. Temporal concatenation gICA was then performed using the MELODIC (78) (version 3.15) toolbox of FSL (version 6.0.3) (http://www.fmrib.ox.ac.uk/fsl). This step was repeated 25 times (77).

Second step: gICA was performed on the concatenation of the 25 gICA results from the first

step.

We repeated these steps, incrementing the total independent component (IC) number from 20 by 5. At the total number of IC = 80, we clearly identified each NOI as described in the Results section and Figure 1.

Within-network analysis

Using the dual regression (79) program implemented in FSL, we first regressed each subject's preprocessed data against the meta-ICA maps created above to obtain subject-specific time courses for each IC. In the second step, we regressed the preprocessed data against subject-specific time courses to obtain subject-specific spatial maps for each IC. The spatial maps of the five NOIs were selected for the statistical analysis of within-network connectivity.

Between-network analysis

Subsequently, we performed TDR (80). After the second step of dual regression, mixture model thresholding was applied to each participant's spatial maps (78). We then regressed the preprocessed data against these thresholded spatial maps to obtain subject-specific time courses. These time courses represented the regions inside the networks, while those of the first step of dual regression represented the whole brain, including the regions outside the networks (80).

Partial correlations between the time courses of NOI-pairs were calculated using FSLNets version 0.6.3, running on MATLAB R2018b (MathWorks), while controlling for the effects of the other three NOIs. The correlation coefficients were Fisher-transformed into Z-scores and used for statistical analysis of between-network connectivity.

Dynamic analysis using ELA

Next, we performed dynamic (29) analysis using ELA (https://github.com/tkEzaki/energy-

landscape-analysis) (37–42). Each time point of the time courses of the five NOIs was binarized into 1 ("activated") or -1 (“deactivated”), depending on whether the value of a time point was above or below the mean of each time course. Since we had five NOIs, the possible activity patterns at each time point were 2^5 = 32 patterns. We concatenated the binarized time-series data of all subjects and calculated the frequency (probability) of each activity pattern. We then fitted the pairwise maximum entropy model to the data to calculate the "energy" of each activity pattern. Figure 2a shows two-dimensional and three-dimensional views of the “energy landscape,” which consists of the energy levels of 32 activity patterns. This energy landscape had two local minima (frequent, low-energy pattern), one with all five NOIs deactivated (activity pattern 1 in state A), while the other with all NOIs activated (activity pattern 32 in state B). Finally, the frequency and transition rate of the brain states were calculated for each subject and then used in statistical analysis.

Harmonization

The difference between sites reportedly showed substantial effects in multisite MRI studies (81–83). Thus, we estimated and removed site effects using an empirical Bayes framework called ComBat (43–45).

For the within-network analysis, we modeled additive (γ) and multiplicative (δ) site effects at each voxel of each site, assuming that all voxels had the same distributions (γ–Gaussian distribution and δ–inverse gamma distribution). The hyperparameters of these distributions were estimated empirically from the data. γ and δ were estimated using conditional posterior means and removed from the voxel values of the spatial maps. The same procedures were performed for the Z-transformed correlation coefficients of the between-network analysis, and the frequency and transition rate of ELA.

Figure 8 illustrates the effects of harmonization. Figure 8a shows the plot of the sum of each voxel's |site mean – overall mean| against each voxel's overall mean and it shows a

substantial reduction of the site effect at each voxel after ComBat. Similarly, Figures 8b and 8c show the plots of the |site mean-overall mean| against each index of interest and show substantial site-effect reduction.

Statistical analysis

Demographic and clinical data were analyzed using SPSS 27 for Windows (IBM). For all imaging analyses, permutation-based non-parametric inference was performed using PALM (version 116) of FSL (84). In each psychosis stage, we performed 1) group comparison and 2) multiple regression analysis with positive symptom severity, of the within-network connectivity, between-network connectivity, and ELA indices. Age, sex, and mean tSNR were used as covariates. Positive symptom severity was indexed by CAARMS "disorder of thought content" + "perceptual abnormalities" in the UHR and PANSS positive scores in the FEP and ChrP. The statistical threshold was $p < 0.05$, controlling for multiple comparisons of

A) Voxel (within-network analysis only): threshold-free cluster enhancement (TFCE) (46) within each NOI.

B) Number of contrasts: two contrasts (HC > PT and PT > HC and positive or negative correlations).

C) Number of networks/indices: five NOIs for within-network analysis, 10 NOI-pairs for between-network analysis, and two indices (frequency and transition rate) for ELA.

Control across the three psychosis stages was not performed since this study could be considered as a series of independent studies at each stage.

We also supplementarily reported at more liberal thresholds of $p < 0.1$, corrected for voxel, contrast, and network/index, and $p < 0.05$, corrected for voxel and contrast.

Effects of medication and psychosis type

We investigated the effect of medication on significant group differences and correlations according to the following principles:

1) In the case of within-network connectivity analyses, the mean value of the significant clusters was extracted and used for investigation. For between-network and dynamic analyses, we used significant network measures.

2) In the case of UHR, we performed group comparisons or correlational analyses after excluding one patient who was administered 50 mg quetiapine. For group comparisons of FEP and ChrP, we compared the above network values between unmedicated and medicated patients. In the case of correlational analyses of FEP and ChrP, we investigated the interaction between medication and positive symptom severity using the above network measures.

3) Age, sex, and tSNR were used as covariates. The statistical threshold was set at $p < 0.05$, corrected for contrast, and for the network/index if more than two networks/indices were found to be significant at each stage.

4) In the case of FEP, we performed the above analyses for the JHU site as well as for all six sites since this site had both unmedicated and medicated FEP patients.

We examined the effect of psychosis type (affective and non-affective psychosis) similarly if we found significant results for FEP. Since the JHU site included both affective and non-affective psychosis patients, we also performed the above analyses for this site.

Effects of comorbidity, smoking and substance use

Since some UHR individuals from the IoPPN site and some FEP patients from the JHU site had comorbid psychiatric disorders, we additionally investigated the effect of comorbidity in the same way as above for the IoPPN and JHU sites.

We also similarly assessed the effect of smoking on the IoPPN, JHU, Kyoto, OSK,

and Tokyo sites, in which information on smoking was available.

Since some UHR patients from the IoPPN site and some FEP patients from the JHU site had experience with substance use, we also investigated its effects for these sites.

References

1. J. M. Pearce, G. Hall, A model for Pavlovian learning: Variations in the effectiveness of conditioned but not of unconditioned stimuli. *Psychol. Rev.* **87**, 532–552 (1980).

2. C. Koch, S. Ullman, Shifts in selective visual attention: towards the underlying neural circuitry. *Hum. Neurobiol.* **4**, 219–227 (1985).

3. M. Matsumoto, O. Hikosaka, Two types of dopamine neuron distinctly convey positive and negative motivational signals. *Nature*. **459**, 837–841 (2009).

4. M. Matsumoto, M. Takada, Distinct Representations of Cognitive and Motivational Signals in Midbrain Dopamine Neurons. *Neuron*. **79**, 1011–1024 (2013).

5. W. Menegas, K. Akiti, R. Amo, N. Uchida, M. Watabe-Uchida, Dopamine neurons projecting to the posterior striatum reinforce avoidance of threatening stimuli. *Nat. Neurosci.* **21**, 1421–1430 (2018).

6. C. F. Zink, G. Pagnoni, M. E. Martin-Skurski, J. C. Chappelow, G. S. Berns, Human striatal responses to monetary reward depend on saliency. *Neuron*. **42**, 509–517 (2004).

7. C. F. Zink, G. Pagnoni, J. Chappelow, M. Martin-Skurski, G. S. Berns, Human striatal activation reflects degree of stimulus saliency. *NeuroImage*. **29**, 977–983 (2006).

8. J. Jensen, A. J. Smith, M. Willeit, A. P. Crawley, D. J. Mikulis, I. Vitcu, S. Kapur, Separate brain regions code for salience vs. valence during reward prediction in humans. *Hum. Brain Mapp.* **28**, 294–302 (2007).

9. J. C. Cooper, B. Knutson, Valence and salience contribute to nucleus accumbens activation. *NeuroImage*. **39**, 538–547 (2008).

10. S. Kapur, Psychosis as a state of aberrant salience: A framework linking biology, phenomenology, and pharmacology in schizophrenia. *Am J Psychiatry*. **160**, 13–23 (2003).

11. T. J. Crow, Positive and negative schizophrenic symptoms and the role of dopamine. *Br. J. Psychiatry*. **137**, 383–386 (1980).

12. P. Fusar-Poli, A. Meyer-Lindenberg, Striatal presynaptic dopamine in schizophrenia,

Part II: Meta-analysis of [18F/11C]-DOPA PET studies. *Schizophr. Bull.* **39**, 33–42 (2013).

13. D. J. Lodge, A. A. Grace, Hippocampal dysregulation of dopamine system function and the pathophysiology of schizophrenia. *Trends Pharmacol. Sci.* **32**, 507–513 (2011).

14. T. Winton-Brown, A. Schmidt, J. P. Roiser, O. D. Howes, A. Egerton, P. Fusar-Poli, N. Bunzeck, A. A. Grace, E. Duzel, S. Kapur, P. McGuire, Altered activation and connectivity in a hippocampal–basal ganglia–midbrain circuit during salience processing in subjects at ultra high risk for psychosis. *Transl. Psychiatry*. **7**, e1245 (2017).

15. G. Modinos, P. Allen, A. Zugman, D. Dima, M. Azis, C. Samson, I. Bonoldi, B. Quinn, G. W. G. Gifford, S. E. Smart, M. Antoniades, M. G. Bossong, M. R. Broome, J. Perez, O. D. Howes, J. M. Stone, A. A. Grace, P. McGuire, Neural circuitry of novelty salience processing in psychosis risk: association with clinical outcome. *Schizophr. Bull.* **46**, 670–679 (2020).

16. W. W. Seeley, V. Menon, A. F. Schatzberg, J. Keller, G. H. Glover, H. Kenna, A. L. Reiss, M. D. Greicius, Dissociable intrinsic connectivity networks for salience processing and executive control. *J. Neurosci.* **27**, 2349–2356 (2007).

17. N. U. F. Dosenbach, D. A. Fair, F. M. Miezin, A. L. Cohen, K. K. Wenger, R. A. T. Dosenbach, M. D. Fox, A. Z. Snyder, J. L. Vincent, M. E. Raichle, B. L. Schlaggar, S. E. Petersen, Distinct brain networks for adaptive and stable task control in humans. *Proc. Natl. Acad. Sci.* **104**, 11073–11078 (2007).

18. T. P. White, V. Joseph, S. T. Francis, P. F. Liddle, Aberrant salience network (bilateral insula and anterior cingulate cortex) connectivity during information processing in schizophrenia. *Schizophr. Res.* **123**, 105–115 (2010).

19. L. Palaniyappan, M. Simmonite, T. P. White, E. B. Liddle, P. F. Liddle, Neural Primacy of the Salience Processing System in Schizophrenia. *Neuron*. **79**, 814–828 (2013).

20. D. Dong, Y. Wang, X. Chang, C. Luo, D. Yao, Dysfunction of Large-Scale Brain Networks in Schizophrenia: A meta-analysis of resting-state functional connectivity. *Schizophr. Bull.* **44**, 168–181 (2018).

21. S. Robinson, G. Basso, N. Soldati, U. Sailer, J. Jovicich, L. Bruzzone, I. Kryspin-Exner, H. Bauer, E. Moser, A resting state network in the motor control circuit of the basal ganglia. *BMC Neurosci.* **10**, 137 (2009).

22. W. R. Shirer, S. Ryali, E. Rykhlevskaia, V. Menon, M. D. Greicius, Decoding subject-driven cognitive states with whole-brain connectivity patterns. *Cereb. Cortex*. **22**, 158–165 (2012).

23. S. A. Meda, A. Gill, M. C. Stevens, R. P. Lorenzoni, D. C. Glahn, V. D. Calhoun, J. A. Sweeney, C. A. Tamminga, M. S. Keshavan, G. Thaker, G. D. Pearlson, Differences in resting-state functional magnetic resonance imaging functional network connectivity between schizophrenia and psychotic bipolar probands and their unaffected first-degree relatives. *Biol. Psychiatry*. **71**, 881–889 (2012).

24. M. S. Ritsner, I. I. Gottesman, in *The Handbook of Neuropsychiatric Biomarkers, Endophenotypes and Genes*, M. S. Ritsner, Ed. (Springer Netherlands, Dordrecht, 2009; http://link.springer.com/10.1007/978-1-4020-9464-4_1), pp. 3–21.

25. R. Khoury, H. A. Nasrallah, Inflammatory biomarkers in individuals at clinical high risk for psychosis (CHR-P): State or trait? *Schizophr. Res.* **199**, 31–38 (2018).

26. Y. Y. Lema, N. J. Gamo, K. Yang, K. Ishizuka, Trait and state biomarkers for psychiatric disorders: Importance of infrastructure to bridge the gap between basic and clinical research and industry. *Psychiatry Clin. Neurosci.* **72**, 482–489 (2018).

27. National Institute of Mental Health Strategic Plan | 2008, 46.

28. B. B. Sheitman, J. A. Lieberman, The natural history and pathophysiology of treatment resistant schizophrenia. *J. Psychiatr. Res.* **32**, 143–150 (1998).

29. R. M. Hutchison, T. Womelsdorf, E. A. Allen, P. A. Bandettini, V. D. Calhoun, M. Corbetta, S. Della Penna, J. H. Duyn, G. H. Glover, J. Gonzalez-Castillo, D. A. Handwerker, S. Keilholz, V. Kiviniemi, D. A. Leopold, F. de Pasquale, O. Sporns, M. Walter, C. Chang, Dynamic functional connectivity: Promise, issues, and interpretations. *NeuroImage*. **80**, 360–378 (2013).

30. Ü. Sakoğlu, G. D. Pearlson, K. A. Kiehl, Y. M. Wang, A. M. Michael, V. D. Calhoun, A

method for evaluating dynamic functional network connectivity and task-modulation: application to schizophrenia. *Magn. Reson. Mater. Phys. Biol. Med.* **23**, 351–366 (2010).

31. A. R. Yung, H. P. Yuen, P. D. McGorry, L. J. Phillips, D. Kelly, M. Dell'Olio, S. M. Francey, E. M. Cosgrave, E. Killackey, C. Stanford, K. Godfrey, J. Buckby, Mapping the onset of psychosis: The comprehensive assessment of at-risk mental states. *Aust. N. Z. J. Psychiatry*. **39**, 964–971 (2005).

32. S. R. Kay, A. Fiszbein, L. A. Opler, The positive and negative syndrome scale (PANSS) for schizophrenia. *Schizophr. Bull.* **13**, 261–276 (1987).

33. T. Aso, G. Jiang, S. Urayama, H. Fukuyama, A Resilient, Non-neuronal Source of the Spatiotemporal Lag Structure Detected by BOLD signal-based blood flow tracking. *Front. Neurosci.* **11** (2017), doi:10.3389/fnins.2017.00256.

34. S. M. Smith, P. T. Fox, K. L. Miller, D. C. Glahn, P. M. Fox, C. E. Mackay, N. Filippini, K. E. Watkins, R. Toro, A. R. Laird, C. F. Beckmann, Correspondence of the brain's functional architecture during activation and rest. *Proc. Natl. Acad. Sci.* **106**, 13040–13045 (2009).

35. B. B. Biswal, M. Mennes, X.-N. Zuo, S. Gohel, C. Kelly, S. M. Smith, C. F. Beckmann, J. S. Adelstein, R. L. Buckner, S. Colcombe, A.-M. Dogonowski, M. Ernst, D. Fair, M. Hampson, M. J. Hoptman, J. S. Hyde, V. J. Kiviniemi, R. Kötter, S.-J. Li, C.-P. Lin, M. J. Lowe, C. Mackay, D. J. Madden, K. H. Madsen, D. S. Margulies, H. S. Mayberg, K. McMahon, C. S. Monk, S. H. Mostofsky, B. J. Nagel, J. J. Pekar, S. J. Peltier, S. E. Petersen, V. Riedl, S. A. R. B. Rombouts, B. Rypma, B. L. Schlaggar, S. Schmidt, R. D. Seidler, G. J. Siegle, C. Sorg, G.-J. Teng, J. Veijola, A. Villringer, M. Walter, L. Wang, X.-C. Weng, S. Whitfield-Gabrieli, P. Williamson, C. Windischberger, Y.-F. Zang, H.-Y. Zhang, F. X. Castellanos, M. P. Milham, Toward discovery science of human brain function. *Proc. Natl. Acad. Sci.* **107**, 4734–4739 (2010).

36. J. D. Bijsterbosch, M. W. Woolrich, M. F. Glasser, E. C. Robinson, C. F. Beckmann, D. C. Van Essen, S. J. Harrison, S. M. Smith, The relationship between spatial configuration and functional connectivity of brain regions. *eLife*. **7**, e32992 (2018).

37. T. Watanabe, S. Hirose, H. Wada, Y. Imai, T. Machida, I. Shirouzu, S. Konishi, Y.

Miyashita, N. Masuda, A pairwise maximum entropy model accurately describes resting-state human brain networks. *Nat. Commun.* **4**, 1370 (2013).

38. T. Watanabe, S. Hirose, H. Wada, Y. Imai, T. Machida, I. Shirouzu, S. Konishi, Y. Miyashita, N. Masuda, Energy landscapes of resting-state brain networks. *Front. Neuroinformatics*. **8** (2014), doi:10.3389/fninf.2014.00012.

39. T. Watanabe, N. Masuda, F. Megumi, R. Kanai, G. Rees, Energy landscape and dynamics of brain activity during human bistable perception. *Nat. Commun.* **5**, 4765 (2014).

40. T. Ezaki, T. Watanabe, M. Ohzeki, N. Masuda, Energy landscape analysis of neuroimaging data. *Phil Trans R Soc A*. **375**, 20160287 (2017).

41. T. Watanabe, G. Rees, Brain network dynamics in high-functioning individuals with autism. *Nat. Commun.* **8**, 16048 (2017).

42. T. Ezaki, M. Sakaki, T. Watanabe, N. Masuda, Age-related changes in the ease of dynamical transitions in human brain activity. *Hum. Brain Mapp.* **39**, 2673–2688 (2018).

43. W. E. Johnson, C. Li, A. Rabinovic, Adjusting batch effects in microarray expression data using empirical Bayes methods. *Biostatistics*. **8**, 118–127 (2007).

44. J.-P. Fortin, D. Parker, B. Tunç, T. Watanabe, M. A. Elliott, K. Ruparel, D. R. Roalf, T. D. Satterthwaite, R. C. Gur, R. E. Gur, R. T. Schultz, R. Verma, R. T. Shinohara, Harmonization of multi-site diffusion tensor imaging data. *NeuroImage*. **161**, 149–170 (2017).

45. M. Yu, K. A. Linn, P. A. Cook, M. L. Phillips, M. McInnis, M. Fava, M. H. Trivedi, M. M. Weissman, R. T. Shinohara, Y. I. Sheline, Statistical harmonization corrects site effects in functional connectivity measurements from multi-site fMRI data. *Hum. Brain Mapp.* **39**, 4213–4227 (2018).

46. S. M. Smith, T. E. Nichols, Threshold-free cluster enhancement: Addressing problems of smoothing, threshold dependence and localisation in cluster inference. *NeuroImage*. **44**, 83–98 (2009).

47. M. Goodkind, S. B. Eickhoff, D. J. Oathes, Y. Jiang, A. Chang, L. B. Jones-Hagata, B. N. Ortega, Y. V. Zaiko, E. L. Roach, M. S. Korgaonkar, S. M. Grieve, I. Galatzer-Levy, P. T. Fox, A. Etkin, Identification of a common neurobiological substrate for mental illness. *JAMA Psychiatry*. **72**, 305–315 (2015).

48. T. T. Winton-Brown, P. Fusar-Poli, M. A. Ungless, O. D. Howes, Dopaminergic basis of salience dysregulation in psychosis. *Trends Neurosci.* **37**, 85–94 (2014).

49. A. V. Faria, Y. Zhao, C. Ye, J. Hsu, K. Yang, E. Cifuentes, L. Wang, S. Mori, M. Miller, B. Caffo, A. Sawa, Multimodal MRI assessment for first episode psychosis: A major change in the thalamus and an efficient stratification of a subgroup. *Hum. Brain Mapp.* **42**, 1034–1053 (2021).

50. Y. Zhu, G. Nachtrab, P. C. Keyes, W. E. Allen, L. Luo, X. Chen, Dynamic salience processing in paraventricular thalamus gates associative learning. *Science*. **362**, 423–429 (2018).

51. C. Sorg, A. Manoliu, S. Neufang, N. Myers, H. Peters, D. Schwerthöffer, M. Scherr, M. Mühlau, C. Zimmer, A. Drzezga, H. Förstl, J. Bäuml, T. Eichele, A. M. Wohlschläger, V. Riedl, Increased intrinsic brain activity in the striatum reflects symptom dimensions in schizophrenia. *Schizophr. Bull.* **39**, 387–395 (2013).

52. M. Duan, X. Chen, H. He, Y. Jiang, S. Jiang, Q. Xie, Y. Lai, C. Luo, D. Yao, Altered basal ganglia network integration in schizophrenia. *Front. Hum. Neurosci.*, 561 (2015).

53. A. Manoliu, V. Riedl, A. Doll, J. G. Bäuml, J. Bäuml, K. Koch, Insular dysfunction reflects altered between-network connectivity and severity of negative symptoms in schizophrenia during psychotic remission. *Front. Hum. Neurosci.* **7**, 216 (2013).

54. A. Manoliu, V. Riedl, A. Zherdin, M. Mühlau, D. Schwerthöffer, M. Scherr, H. Peters, C. Zimmer, H. Förstl, J. Bäuml, A. M. Wohlschläger, C. Sorg, Aberrant dependence of default mode/central executive network interactions on anterior insular salience network activity in schizophrenia. *Schizophr. Bull.* **40**, 428–437 (2014).

55. Y. Wang, W. Tang, X. Fan, J. Zhang, D. Geng, K. Jiang, D. Zhu, Z. Song, Z. Xiao, D. Liu, Resting-state functional connectivity changes within the default mode network and the salience network after antipsychotic treatment in early-phase schizophrenia.

Neuropsychiatr. Dis. Treat. Volume **13**, 397–406 (2017).

56. M. Ohta, M. Nakataki, T. Takeda, S. Numata, T. Tominaga, N. Kameoka, H. Kubo, M. Kinoshita, K. Matsuura, M. Otomo, N. Takeichi, M. Harada, T. Ohmori, Structural equation modeling approach between salience network dysfunction, depressed mood, and subjective quality of life in schizophrenia: an ICA resting-state fMRI study. *Neuropsychiatr. Dis. Treat.* (2018), , doi:10.2147/NDT.S163132.

57. F. Orliac, M. Naveau, M. Joliot, N. Delcroix, A. Razafimandimby, P. Brazo, S. Dollfus, P. Delamillieure, Links among resting-state default-mode network, salience network, and symptomatology in schizophrenia. *Schizophr. Res.* **148**, 74–80 (2013).

58. X. Wang, W. Zhang, Y. Sun, M. Hu, A. Chen, Aberrant intra-salience network dynamic functional connectivity impairs large-scale network interactions in schizophrenia. *Neuropsychologia*. **93**, Part A, 262–270 (2016).

59. K. Supekar, W. Cai, R. Krishnadas, L. Palaniyappan, V. Menon, Dysregulated brain dynamics in a triple-network saliency model of schizophrenia and its relation to psychosis. *Biol. Psychiatry*. **85**, 60–69 (2019).

60. J. Miyata, Toward integrated understanding of salience in psychosis. *Neurobiol. Dis.* (2019), doi:10.1016/j.nbd.2019.03.002.

61. A. Demjaha, J. M. Lappin, D. Stahl, M. X. Patel, J. H. MacCabe, O. D. Howes, M. Heslin, U. A. Reininghaus, K. Donoghue, B. Lomas, M. Charalambides, A. Onyejiaka, P. Fearon, P. Jones, G. Doody, C. Morgan, P. Dazzan, R. M. Murray, Antipsychotic treatment resistance in first-episode psychosis: prevalence, subtypes and predictors. *Psychol. Med.* **47**, 1981–1989 (2017).

62. B. T. T. Yeo, F. M. Krienen, J. Sepulcre, M. R. Sabuncu, D. Lashkari, M. Hollinshead, J. L. Roffman, J. W. Smoller, L. Zöllei, J. R. Polimeni, B. Fischl, H. Liu, R. L. Buckner, The organization of the human cerebral cortex estimated by intrinsic functional connectivity. *J. Neurophysiol.* **106**, 1125–1165 (2011).

63. J. D. Power, A. L. Cohen, S. M. Nelson, G. S. Wig, K. A. Barnes, J. A. Church, A. C. Vogel, T. O. Laumann, F. M. Miezin, B. L. Schlaggar, S. E. Petersen, Functional network organization of the human brain. *Neuron*. **72**, 665–678 (2011).

64. S. L. Bressler, V. Menon, Large-scale brain networks in cognition: emerging methods and principles. *Trends Cogn. Sci.* **14**, 277–290 (2010).

65. V. Menon, L. Q. Uddin, Saliency, switching, attention and control: a network model of insula function. *Brain Struct. Funct.* **214**, 655–667 (2010).

66. M. F. Glasser, T. S. Coalson, E. C. Robinson, C. D. Hacker, J. Harwell, E. Yacoub, K. Ugurbil, J. Andersson, C. F. Beckmann, M. Jenkinson, S. M. Smith, D. C. Van Essen, A multi-modal parcellation of human cerebral cortex. *Nature*. **536**, 171–178 (2016).

67. A. M. Wang, S. Pradhan, J. M. Coughlin, A. Trivedi, S. L. DuBois, J. L. Crawford, T. W. Sedlak, F. C. Nucifora, G. Nestadt, L. G. Nucifora, D. J. Schretlen, A. Sawa, P. B. Barker, Assessing brain metabolism with 7-T proton magnetic resonance spectroscopy in patients with first-episode psychosis. *JAMA Psychiatry* (2019), doi:10.1001/jamapsychiatry.2018.3637.

68. V. Kamath, P. Lasutschinkow, K. Ishizuka, A. Sawa, Olfactory Functioning in First-Episode Psychosis. *Schizophr. Bull.* **44**, 672–680 (2018).

69. A. V. Faria, J. Crawford, C. Ye, J. Hsu, A. Kenkare, D. Schretlen, A. Sawa, Relationship between neuropsychological behavior and brain white matter in first-episode psychosis. *Schizophr. Res.* (2019), doi:10.1016/j.schres.2019.04.010.

70. N. C. Andreasen, *Scale for the assessment of positive symptoms: SAPS* (University of Iowa, 1984).

71. N. C. Andreasen, *Scale for the Assessment of Negative Symptoms* (University of Iowa, 1981).

72. T. G. M. van Erp, A. Preda, D. Nguyen, L. Faziola, J. Turner, J. Bustillo, A. Belger, K. O. Lim, S. McEwen, J. Voyvodic, D. H. Mathalon, J. Ford, S. G. Potkin, Fbirn, Converting positive and negative symptom scores between PANSS and SAPS/SANS. *Schizophr. Res.* **152**, 289–294 (2014).

73. M. Jenkinson, P. Bannister, M. Brady, S. Smith, Improved Optimization for the Robust and Accurate Linear Registration and Motion Correction of Brain Images. *NeuroImage*. **17**, 825–841 (2002).

74. L. Griffanti, G. Salimi-Khorshidi, C. F. Beckmann, E. J. Auerbach, G. Douaud, C. E. Sexton, E. Zsoldos, K. P. Ebmeier, N. Filippini, C. E. Mackay, S. Moeller, J. Xu, E. Yacoub, G. Baselli, K. Ugurbil, K. L. Miller, S. M. Smith, ICA-based artefact removal and accelerated fMRI acquisition for improved resting state network imaging. *NeuroImage*. **95**, 232–247 (2014).

75. G. Salimi-Khorshidi, G. Douaud, C. F. Beckmann, M. F. Glasser, L. Griffanti, S. M. Smith, Automatic denoising of functional MRI data: Combining independent component analysis and hierarchical fusion of classifiers. *NeuroImage*. **90**, 449–468 (2014).

76. D. R. Roalf, M. Quarmley, M. A. Elliott, T. D. Satterthwaite, S. N. Vandekar, K. Ruparel, E. D. Gennatas, M. E. Calkins, T. M. Moore, R. Hopson, K. Prabhakaran, C. T. Jackson, R. Verma, H. Hakonarson, R. C. Gur, R. E. Gur, The impact of quality assurance assessment on diffusion tensor imaging outcomes in a large-scale population-based cohort. *NeuroImage*. **125**, 903–919 (2016).

77. A. B. Poppe, K. Wisner, G. Atluri, K. O. Lim, V. Kumar, A. W. MacDonald, Toward a neurometric foundation for probabilistic independent component analysis of fMRI data. *Cogn. Affect. Behav. Neurosci.* **13**, 641–659 (2013).

78. C. F. Beckmann, S. M. Smith, Probabilistic independent component analysis for functional magnetic resonance imaging. *IEEE Trans. Med. Imaging*. **23**, 137–152 (2004).

79. N. Filippini, B. J. MacIntosh, M. G. Hough, G. M. Goodwin, G. B. Frisoni, S. M. Smith, P. M. Matthews, C. F. Beckmann, C. E. Mackay, Distinct patterns of brain activity in young carriers of the APOE-ε4 allele. *Proc. Natl. Acad. Sci.* **106**, 7209–7214 (2009).

80. J. D. Bijsterbosch, C. F. Beckmann, M. W. Woolrich, S. M. Smith, S. J. Harrison, The relationship between spatial configuration and functional connectivity of brain regions revisited. *eLife*. **8**, e44890 (2019).

81. A. Yamashita, N. Yahata, T. Itahashi, G. Lisi, T. Yamada, N. Ichikawa, M. Takamura, Y. Yoshihara, A. Kunimatsu, N. Okada, H. Yamagata, K. Matsuo, R. Hashimoto, G. Okada, Y. Sakai, J. Morimoto, J. Narumoto, Y. Shimada, K. Kasai, N. Kato, H. Takahashi, Y. Okamoto, S. C. Tanaka, M. Kawato, O. Yamashita, H. Imamizu, Harmonization of

resting-state functional MRI data across multiple imaging sites via the separation of site differences into sampling bias and measurement bias. *PLOS Biol.* **17**, e3000042 (2019).

82. Y. Yoshihara, G. Lisi, N. Yahata, J. Fujino, Y. Matsumoto, J. Miyata, G. Sugihara, S. Urayama, M. Kubota, M. Yamashita, R. Hashimoto, N. Ichikawa, W. Cahn, N. E. M. van Haren, S. Mori, Y. Okamoto, K. Kasai, N. Kato, H. Imamizu, R. S. Kahn, A. Sawa, M. Kawato, T. Murai, J. Morimoto, H. Takahashi, Overlapping but asymmetrical relationships between schizophrenia and autism revealed by brain connectivity. *Schizophr. Bull.* **46**, 1210–1218 (2020).

83. Y. Mori, J. Miyata, M. Isobe, S. Son, Y. Yoshihara, T. Aso, T. Kouchiyama, T. Murai, H. Takahashi, Effect of phase-encoding direction on group analysis of resting-state functional magnetic resonance imaging. *Psychiatry Clin. Neurosci.* **72**, 683–691 (2018).

84. A. M. Winkler, M. A. Webster, J. C. Brooks, I. Tracey, S. M. Smith, T. E. Nichols, Non-parametric combination and related permutation tests for neuroimaging: NPC and Related Permutation Tests for Neuroimaging. *Hum. Brain Mapp.* **37**, 1486–1511 (2016).

85. R. Suurmond, H. van Rhee, T. Hak, Introduction, comparison, and validation of Meta-Essentials: A free and simple tool for meta-analysis. *Res. Synth. Methods*. **8**, 537–553 (2017).

Acknowledgments

The authors wish to extend their gratitude to the patients and volunteers for their participation in this study. They also thank all the lab and COCORO consortium members for their contributions and Editage (www.editage.com) for English language editing.

Funding

This work was supported by the following funding sources.

JSPS/MEXT KAKENHI grant 26461767 (JM)

JSPS/MEXT KAKENHI grant 17H04248 (JM)

JSPS/MEXT KAKENHI grant 18H05130 (JM)

JSPS/MEXT KAKENHI grant 20H05064 (JM)

JSPS/MEXT KAKENHI grant 19H03583 (HT)

JSPS/MEXT KAKENHI grant 23120009 (HT)

JSPS/MEXT KAKENHI grant 16H06572 (HT)

JSPS/MEXT KAKENHI grant 20K21567 (HT)

JSPS/MEXT KAKENHI grant 15H04893 (TM)

JSPS/MEXT KAKENHI grant 16H06397 (TM)

JSPS/MEXT KAKENHI grant JP16H06280 (KK)

JSPS/MEXT KAKENHI grant JP18K07550 (TT)

JSPS/MEXT KAKENHI grant JP21K12153 (KN)

JST ImPACT grant 15808865 (TM)

JST Moonshot R&D grant JPMJMS2021 (SK and KK)

grants from the Japan Foundation for Aging and Health (HT)

AMED Strategic Research Program for Brain Sciences grant 17dm0107044h0005 (HT)

AMED Strategic Research Program for Brain Sciences grant 20dm0107088h0005 (TM)

AMED Brain/MINDS & beyond grant 21dm0307008h0004 (JM, HT)

AMED Brain/MINDS & beyond grant 20dm0307102h0002 (TM)

AMED Brain/MINDS & beyond grant JP21dm0307001 (KK)

AMED Brain/MINDS & beyond grant JP21dm020769 (KK)

AMED Brain/MINDS & beyond grant JP21dm0307004 (SK and KK)

AMED Brain/MINDS & beyond grant JP21dm0307002 (RH)

AMED Brain Mapping by Integrated Neurotechnologies for Disease Studies JP20dm0207069 (SK and KK)

AMED grant JP21dk0307103 (RH)

AMED grant JP21uk1024002 (RH)

Intramural Research Grant (3-1) for Neurological and Psychiatric Disorders of NCNP (RH)
Novartis Pharma Research Grant (JM)
a grant from SENSHIN Medical Research Foundation (JM, HT)
a grant from SUZUKEN Memorial Foundation (JM)
Tanabe-Mitsubishi Pharma Research Grant (JM)
a grant from Uehara memorial foundation
Kyoto University Global Frontier Project for Young Professionals (JM)
Takeda Science Foundation (JM and HT)
Kobayashi Magobei Memorial Foundation (HT)
Smoking Research Foundation (HT)
the Kato Memorial Trust for Nambyo Research (TM)
the National Institute of Mental Health (NIMH) grant number MH-094268 (AS)
the National Institute of Mental Health (NIMH) grant number MH-092443 (AS)
the National Institute of Mental Health (NIMH) grant number MH-105660 (AS)
Silvio O. Conte Center funded by NIMH (AS)
the National Institute of Health grant number P41EB015909 (SM)
the National Institute of Health grant number R01NS084957 (SM)
grants from Stanley (AS)
S-R/RUSK (AS)
NARSAD (AS)
Some part of the participant recruitment supported by the Tanabe Mitsubishi Pharm. Co. Ltd. (AS)
Wellcome Trust fellowship grant WT087779MA (TWB)

Author contributions

Conceptualization: JM
Methodology: JM, TA, NAC, TE, TK, NM, KN, and YS.
Data acquisition: JM, TWB, TS, NC, JC, CH, MI, KK (Kouhei Kamiya), KK (Kiyoto Kasai), SK, AK, NM, SM, YM, TM, FN, KO, NO, TT, SU, YW, CCW, HY, YY, RH, HT, AS, and PM.
Investigation: JM
Visualization: JM
Supervision: TWB, NAC, RH, HT, AS, PM
Writing (original draft): JM
Writing (review & editing): JM and all the 36 coauthors

Competing interests

All the authors declare they have no competing interests.

Data and material availability

All data needed to evaluate the conclusions in the paper are present in the paper and/or supplementary materials. Neuroimaging and clinical data and in-house written codes can be provided after scientific review and material transfer agreements. The requests should be submitted to JM.

Figure 1. Five networks of interest (NOIs) from meta-ICA

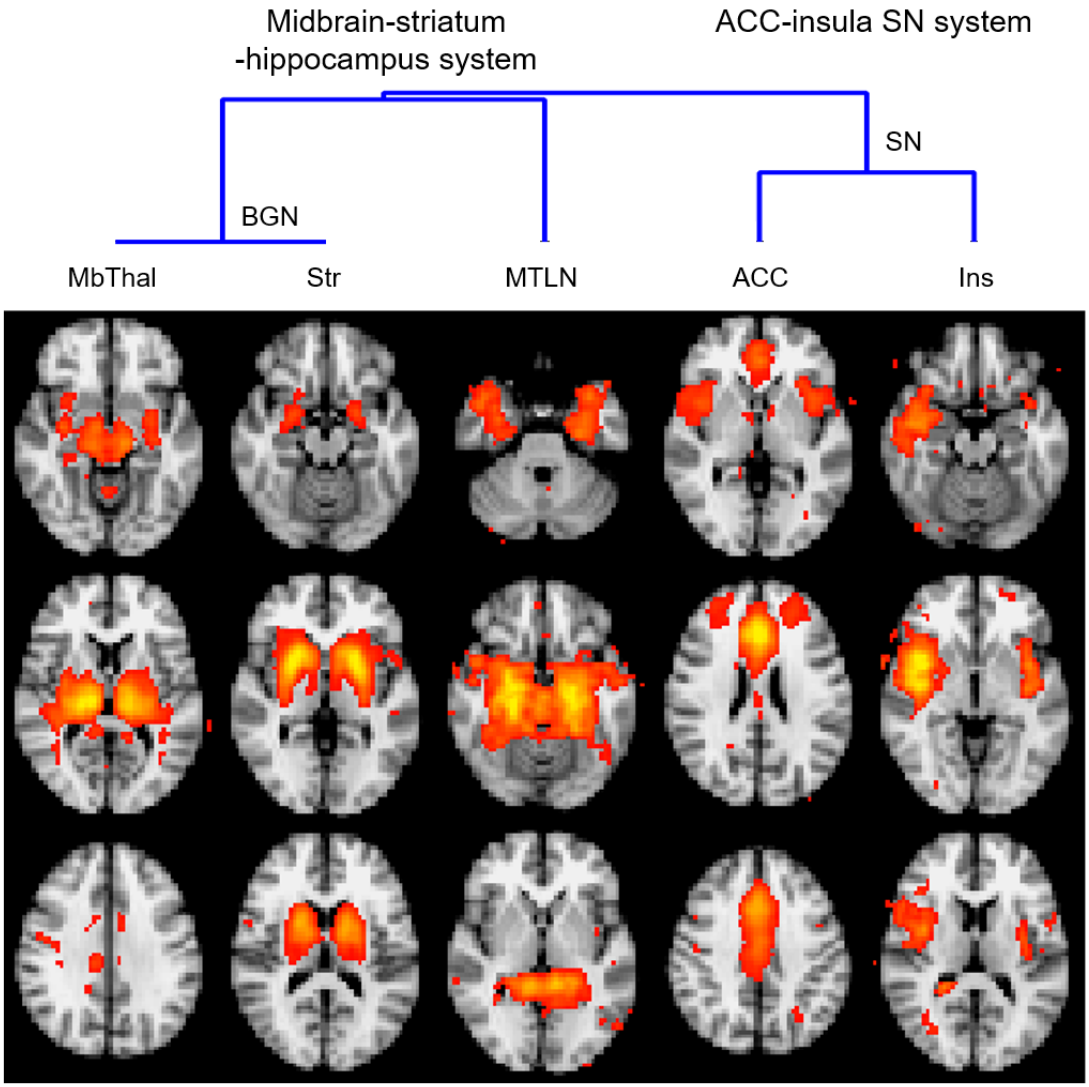

Meta-ICA identified the midbrain-striatum-hippocampus system as the midbrain-thalamus part of the basal ganglia network (BGN-MbThal), the striatum part of the BGN (BGN-Str), and the medial temporal lobe network (MTLN). The analysis also identified the ACC (SN-ACC) and bilateral insula (SN-Ins) regions of the ACC-insula SN system. The results were thresholded at $P > 0.5$, using alternative hypothesis testing in a Gaussian/Gamma mixture model. The hierarchical clustering of networks based on time courses separated each system, and each subnetwork was found to be close to each other.

Abbreviations

ACC, anterior cingulate cortex; ICA, independent component analysis; SN, salience network.

Figure 2. Energy landscape of the five networks of interests (NOIs)

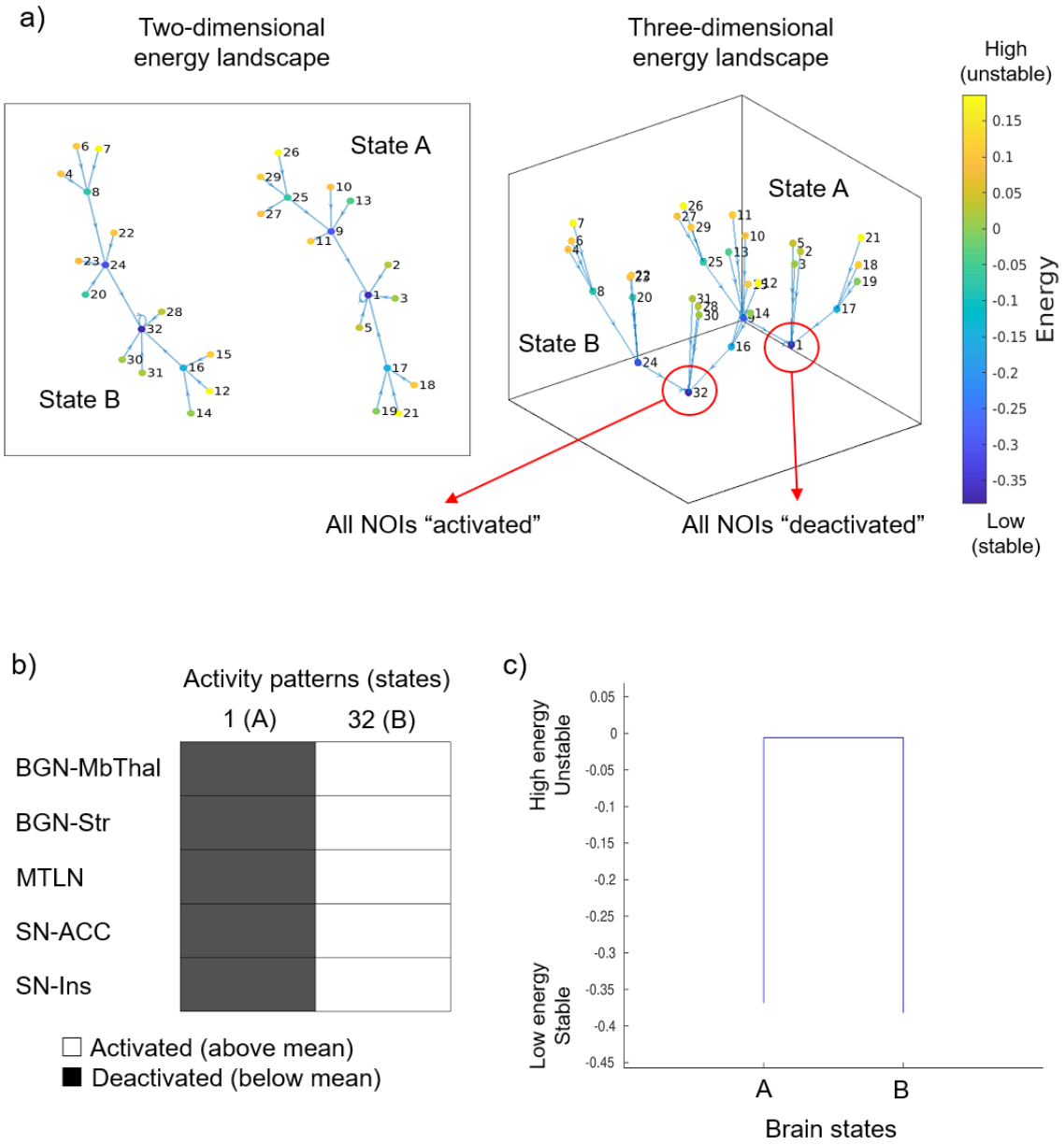

a) Energy landscape analysis classified $2^5 = 32$ "activity" patterns of five NOIs into two brain states.

b) The brain state A was characterized by the local minima (activity pattern 1) where all five NOIs were deactivated (below the mean), while the brain state B had the local minima (activity pattern 32) of all five NOIs activated (above the mean). Yellow indicates high-energy, low-frequency patterns and blue indicates low-energy, high-frequency patterns.

c). Two brain states were with low energy (stable).

Abbreviations

ACC, anterior cingulate cortex; BGN, basal ganglia network; Ins, insula; MbThal, midbrain and thalamus; MTLN, medial temporal lobe network; SN, salience network; Str, striatum.

Figure 3. Group comparison results

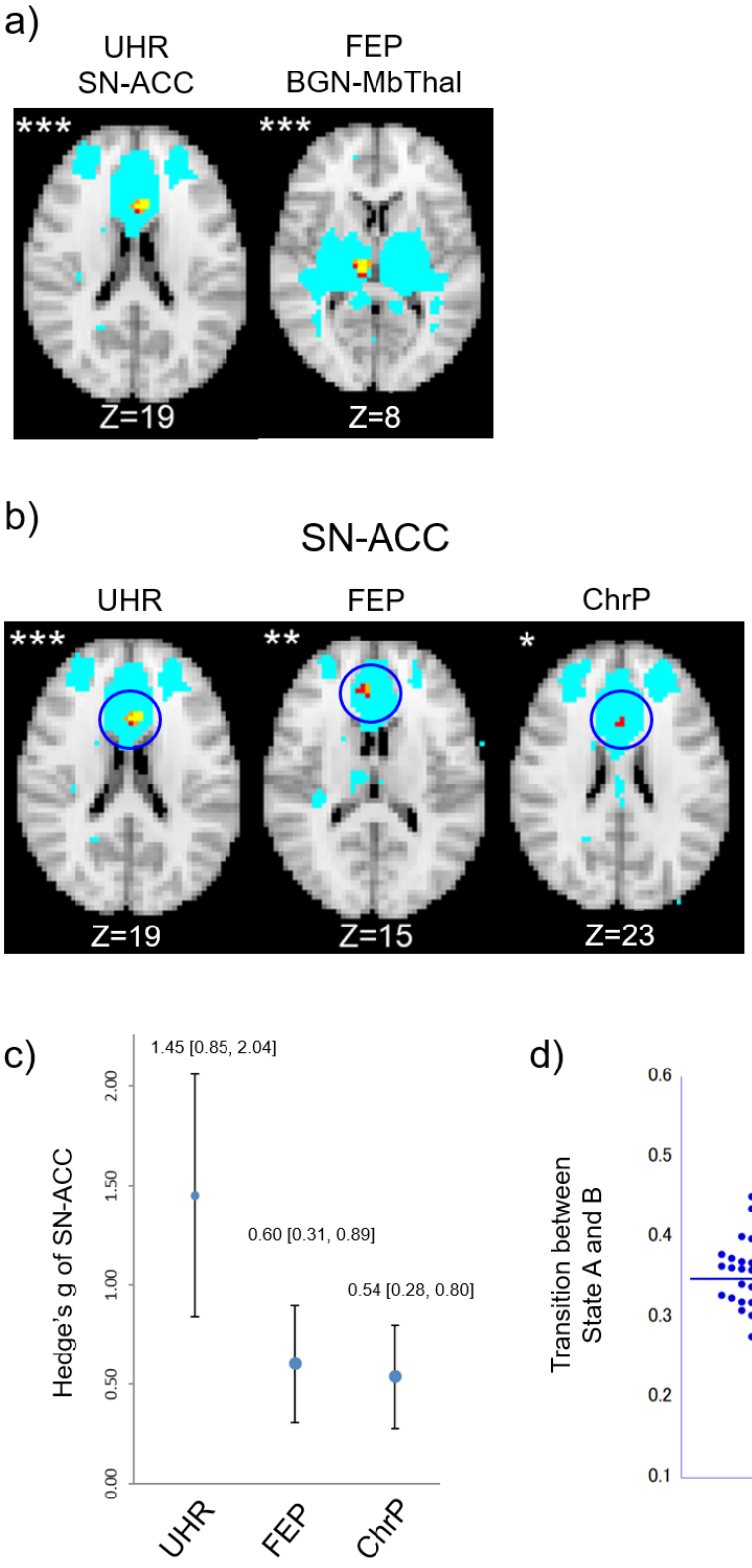

a) Reduced within-network connectivity of the SN-ACC in UHR and BGN-MbThal in FEP patients.

UHR (n=29) patients were compared to matched HC (n=25), FEP (n=81) with matched HC (n=109), and ChrP (n= 99) with matched HC (n=145). Yellow and *** indicate a significant reduction of connectivity in patients at $p < 0.05$, corrected for voxels (threshold-free cluster enhancement), two contrasts (HC > PT and HC < PT), and five networks. Orange and ** indicate trend-level significance at $p < 0.1$, corrected for voxel, contrast, and network. Red and * indicate significance at $p < 0.05$, corrected for voxel and contrast. Light blue indicates the NOIs.

b) The significance of the SN-ACC was UHR > FEP > ChrP.

The ACC clusters were located at almost the same location at each psychosis stage. Yellow and *** indicate a significant reduction of connectivity in patients at $p < 0.05$, corrected for voxel, contrast, and network. Orange and ** indicate trend-level significance at $p < 0.1$, corrected for voxel, contrast, and network. Red and * indicate significance at $p < 0.05$, corrected for voxel and contrast. Light blue indicates the NOIs.

c) The effect size of the ACC cluster was UHR > FEP > ChrP.

Hedge's g scores for UHR, FEP, and ChrP, respectively. A plot was created using Meta-Essentials (*85*).

d) Increased transition between brain states in FEP compared to HC

The statistical threshold was set at $p < 0.05$, corrected for two contrasts and two indices. Brain state A was characterized by the local minima where all five NOIs were deactivated (below the mean), whereas brain state B had the local minima of all five NOIs activated (above the mean).

Abbreviations

ACC, anterior cingulate cortex; BGN, basal ganglia network; ChrP, chronic schizophrenia; FEP, first-episode psychosis; HC, healthy controls; Ins, insula; MbThal, midbrain and thalamus; MTLN, medial temporal lobe network; NOI, network of interest; PT, patients; SN, salience network; Str, striatum; UHR, ultra high risk.

Figure 4

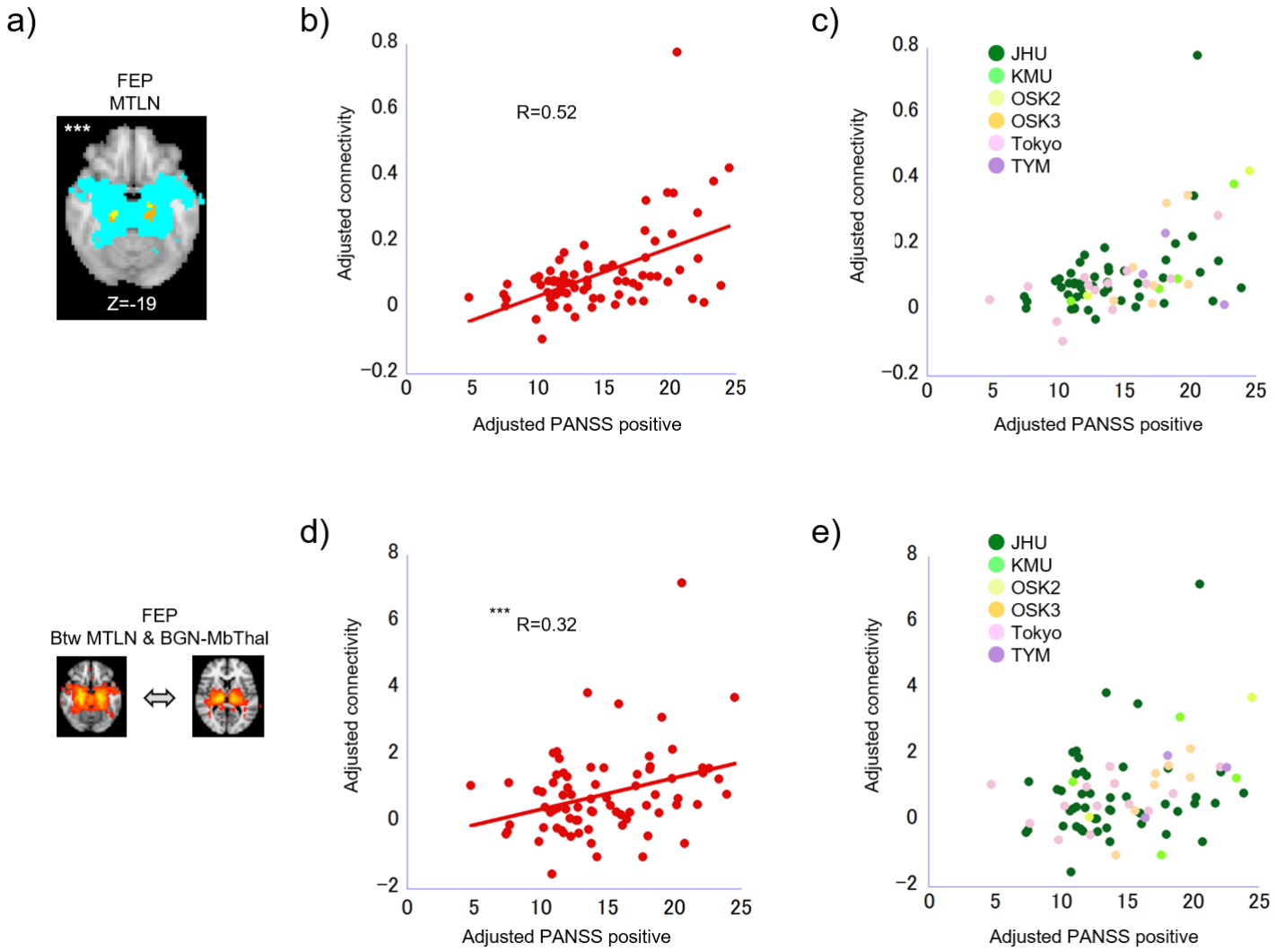

a) Positive correlation between PANSS positive scale and the connectivity within the MTLN in FEP (n = 76).

Yellow and *** indicate significance at $p < 0.05$, corrected for voxels using threshold-free cluster enhancement, two contrasts (HC > PT and HC < PT), and five networks. Orange indicates trend-level significance at $p < 0.1$, corrected for voxel, contrast and network. Light blue indicates the NOI.

b) Scatter plot of a).

PANSS positive scale and connectivity values were adjusted for age, sex, and tSNR.

c) Scatter plot of a) according to site.

There was no clear deviation by site.

d) Scatter plot of the positive correlation between PANSS positive scale and the connectivity between the MTLN and BGN-MbThal in FEP (n = 76).

*** indicates significance at $p < 0.05$, corrected for two contrasts (positive and negative correlations) and 10 NOI-pairs. The PANSS positive scale and connectivity values were adjusted for age, sex, and tSNR.

e) Scatter plot according to each site.

There was no clear deviation by site.

Abbreviations

BGN, basal ganglia network; Btw, between; FEP, first-episode psychosis; MbThal, midbrain and thalamus; MTLN, medial temporal lobe network; NOI, network of interest; PANSS, positive and negative syndrome scale; tSNR, temporal signal-to-noise ratio.

Figure 5

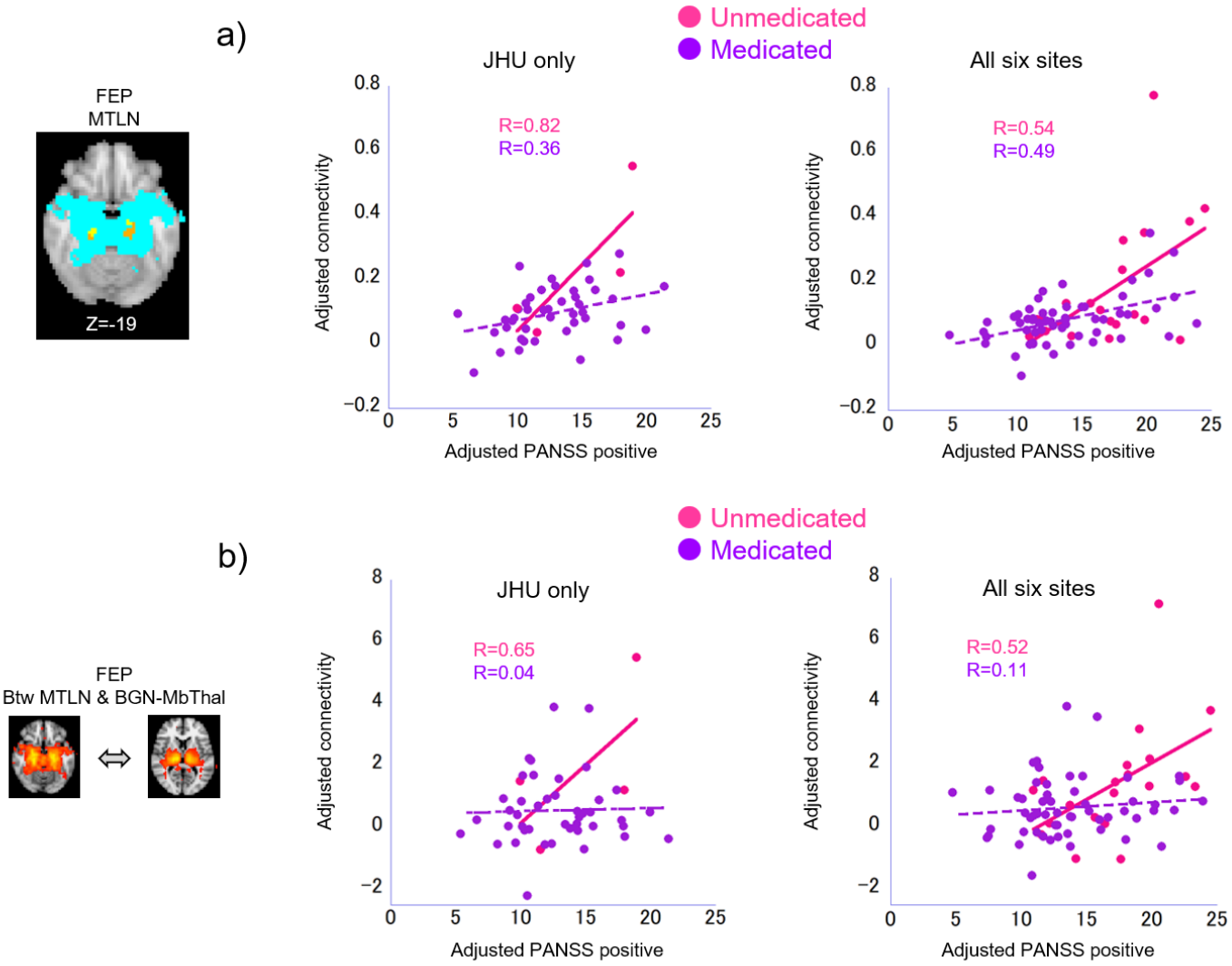

a) Interactions between medication and PANSS positive score on the connectivity within the MTLN in FEP.

Left: At the JHU site (n = 47), the regression slope was steeper in unmedicated (n = 4, magenta) than in medicated (n = 43, purple) FEP patients. Significance level was set at $p < 0.05$, corrected for contrast. PANSS positive scale and connectivity values were adjusted for age, sex, and tSNR. Right: At all six sites (n = 76), the regression slope was steeper in unmedicated (n = 20) than in medicated (n = 56) patients with FEP. Significance level was set at $p < 0.05$, corrected for contrast.

b) Interactions between medication and PANSS positive score on the connectivity between the MTLN and BGN-MbThal in FEP.

Left: At the JHU site (n = 47), the regression slope was steeper in unmedicated (n = 4, magenta) than in medicated (n = 43, purple) FEP patients. Significance level was set at $p < 0.05$, corrected for contrast. PANSS positive scale and connectivity values were adjusted for age, sex, and tSNR. Right: At all six sites (n = 76), the regression slope was steeper in unmedicated (n = 20) than in medicated (n = 56) patients with FEP. Significance level was set at $p < 0.05$, corrected for contrast.

Abbreviations

BGN-MbThal, midbrain and thalamus part of the basal ganglia network; Btw, between; FEP, first-episode psychosis; JHU, Johns Hopkins University; MTLN, medial temporal lobe network; PANSS, positive and negative syndrome scale; tSNR, temporal signal-to-noise ratio.

Figure 6

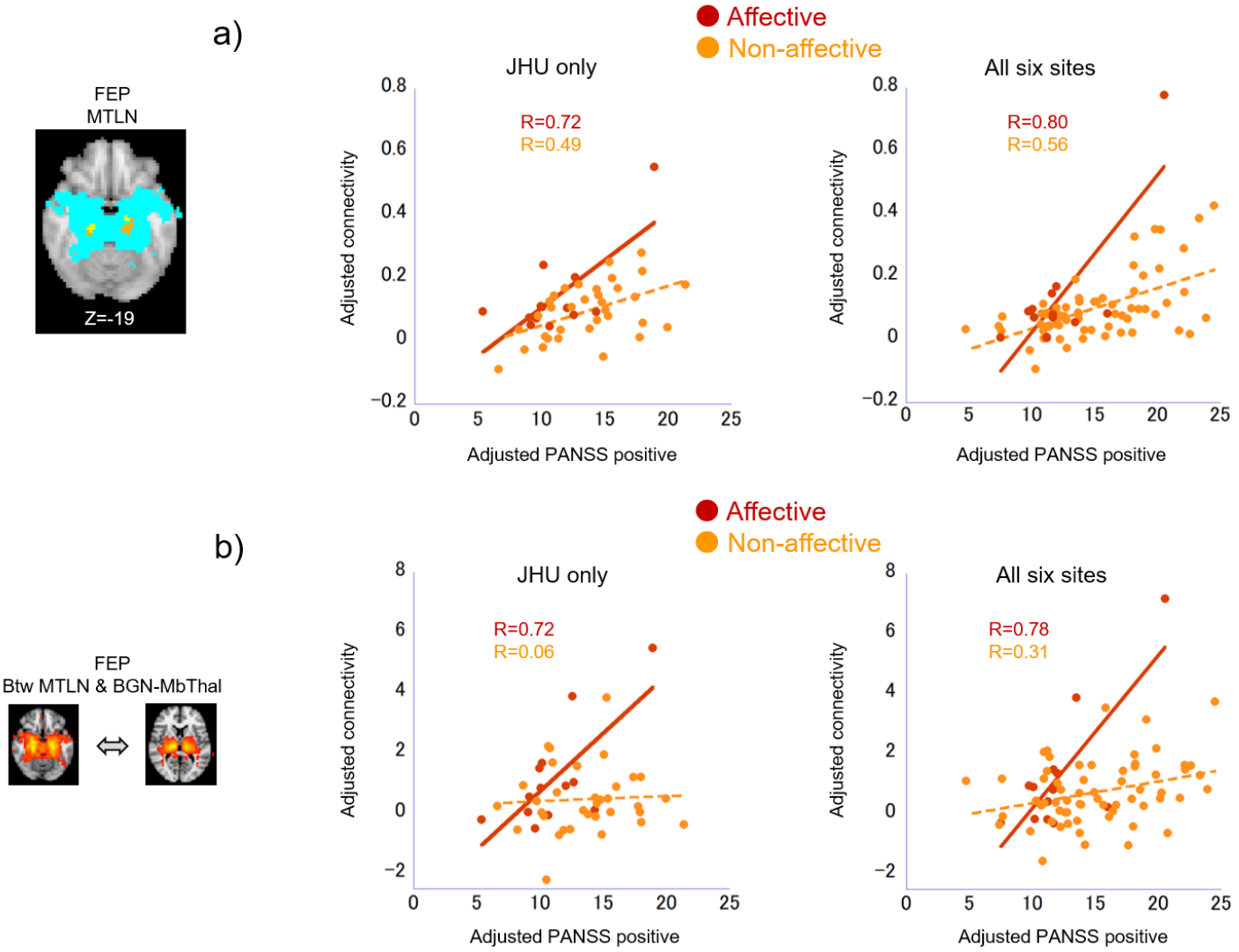

a) Interactions between psychosis type and PANSS positive score on the connectivity within the MTLN in FEP.

Left: At the JHU site (n = 47), the regression slope was steeper in the affective (n = 13, brown) than in the non-affective (n = 34, orange) FEP. Significance level was set at $p < 0.05$, corrected for contrast. PANSS positive scale and connectivity values were adjusted for age, sex, and tSNR. Right: At all six sites (n = 76), the regression slope was steeper in the affective (n = 13) than in the non-affective (n = 63) FEP. Significance level was set at $p < 0.05$, corrected for contrast.

b) Interactions between psychosis type and PANSS positive score on the connectivity between the MTLN and BGN-MbThal in FEP.

Left: At the JHU site (n = 47), the regression slope was steeper in the affective (n = 13, brown) than in the non-affective (n = 34, orange) FEP. Significance level was set at $p < 0.05$, corrected for contrast. PANSS positive scale and connectivity values were adjusted for age, sex, and tSNR. Right: At all six sites (n = 76), the regression slope was steeper in the affective (n = 13) than in the non-affective (n = 63) FEP. Significance level was set at $p < 0.05$, corrected for contrast.

Abbreviations

BGN-MbThal, midbrain and thalamus part of the basal ganglia network; Btw, between; FEP, first-episode psychosis; JHU, Johns Hopkins University; MTLN, medial temporal lobe network; PANSS, positive and negative syndrome scale; tSNR, temporal signal-to-noise ratio.

Figure 7

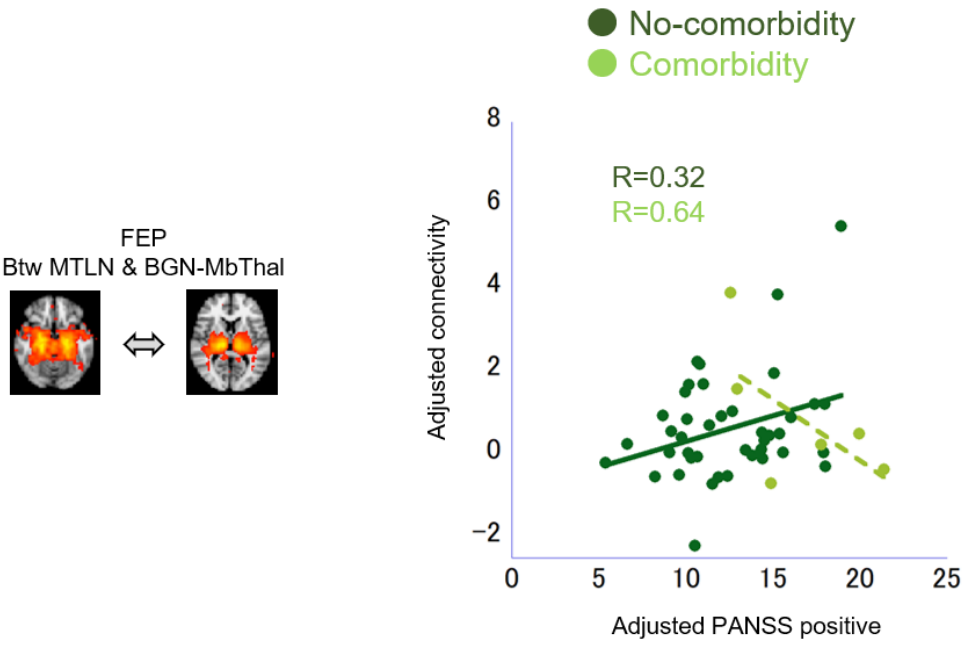

Interaction between comorbidity and PANSS positive score on the connectivity between the MTLN and BGN-MbThal in FEP (JHU site only).

Subanalysis showed a trend-level positive correlation in patients without comorbidity (n = 41, green, p = 0.06, corrected for contrast), whereas no correlation was found in patients with comorbidity (n = 6, light green, p = 0.28, corrected for contrast). PANSS positive scale and connectivity values were adjusted for age, sex, and tSNR.

Abbreviations

BGN-MbThal, midbrain and thalamus part of the basal ganglia network; Btw, between; FEP, first-episode psychosis; JHU, Johns Hopkins University; MTLN, medial temporal lobe network; PANSS, positive and negative syndrome scale; tSNR, temporal signal-to-noise ratio.

Figure 8. ICA-denoising efficiently classified neuronal and noise components.

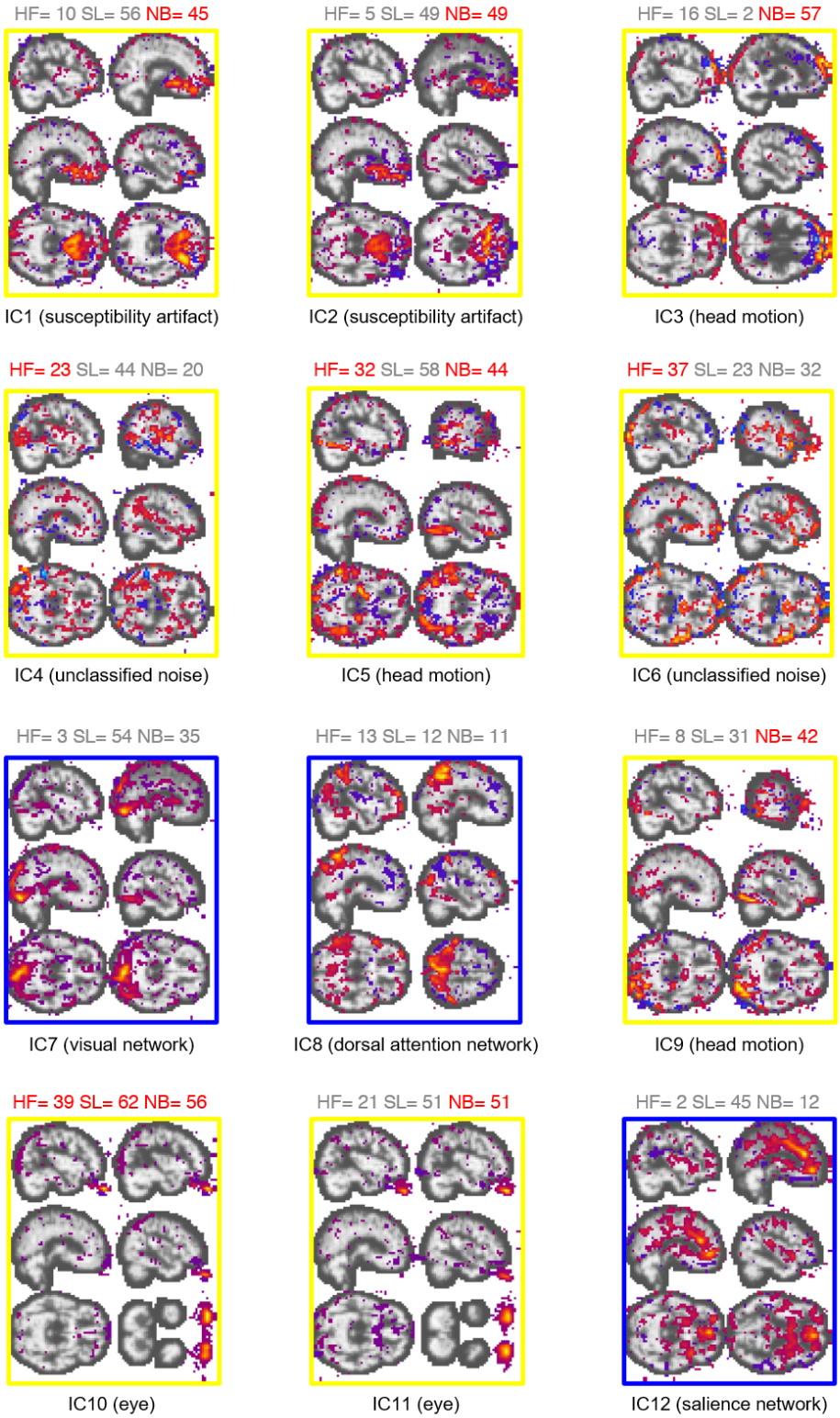

After ICA was applied to each subject's rsfMRI data, the independent components (ICs) were classified as noise based on the following three criteria:

1) high-frequency power ratio (>0.1 Hz up to 0.2 Hz or the Nyquist frequency for the TR) relative to <0.1 Hz (HF)

2) non-gray matter involvement index (NB)

3) slice dependency index calculated as the ratio of within- and between-slice spatial high-frequency components (SL)

The ICs with the top 12 variances of an example subject are shown. The ICs surrounded by blue frames are neuronal components, and the ICs with yellow frames are noise components. The numbers are ranked among all 62 components of this subject, indicating that the smaller the rank, the better. The ranks in red indicate classification into noise.

Abbreviations

ICA, independent component analysis; rsfMRI, resting state functional magnetic resonance imaging.

Figure 9. Harmonization by ComBat effectively removed site-effects.

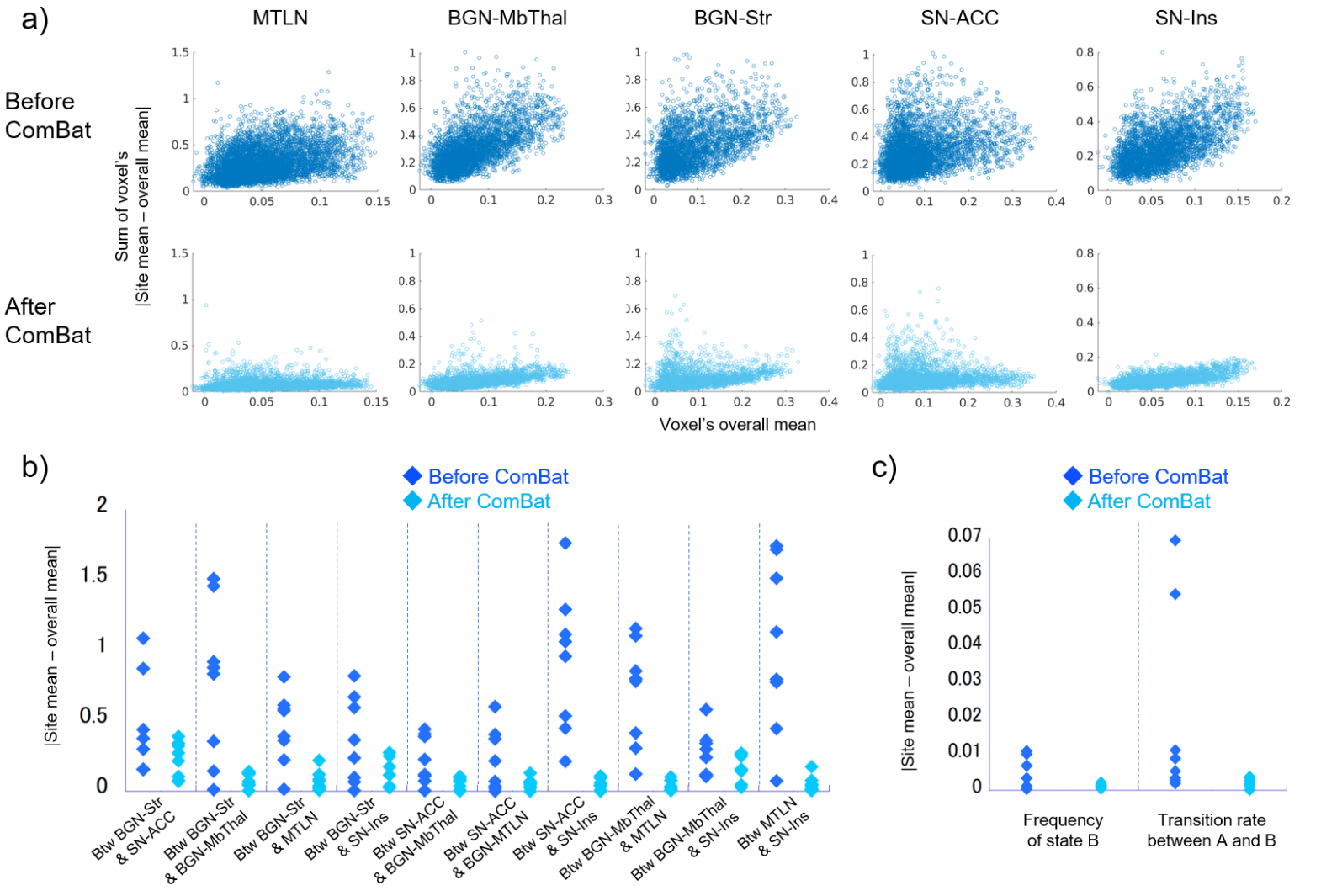

a) Effect of ComBat on the spatial maps of the within-network connectivity analysis.

The sum of each voxel's |site mean − overall mean| was plotted against each voxel's overall mean, controlling for age, sex, and tSNR.

b) Effect of ComBat on the Z-transformed partial correlation coefficients of the between-network connectivity analysis.

The |site mean-overall mean| of the correlation coefficients was plotted for each NOI-pair, controlling for age, sex, and tSNR.

c) Effect of ComBat on the frequency of state B and transition rate between states A and B of the energy landscape analysis.

The |site mean-overall mean| of each index was plotted, controlling for age, sex, and tSNR.

Abbreviations

ACC, anterior cingulate cortex; BGN, basal ganglia network; Btw, between; Ins, insula; MbThal, midbrain and thalamus; MTLN, medial temporal lobe network; SN, salience network; Str, striatum; tSNR, temporal signal-to-noise ratio.

Table 1. Demographic and clinical characteristics of the participants.[a]

	UHR		FEP		ChrP		Total	
Site	HC	PT (Unmed)	HC	PT (Unmed)	HC	PT (Unmed)	HC	PT (Unmed)
IoPPN	25	29 (28)					25	29 (28)
JHU			73	51 (4)			73	51 (4)
KMU			6	4 (4)	9	4 (4)	15	8 (8)
Kyoto					41	46 (0)	41	46 (0)
OSK2			4	2 (2)	13	7 (7)	17	9 (9)
OSK3			11	7 (7)	24	14 (14)	35	21 (21)
Tokyo			10	14 (0)	53	26 (0)	63	40 (0)
TYM			5	3 (3)	5	2 (2)	10	5 (5)
Total	25	29 (28)	109	81 (20)	145	99 (27)	279	209 (75)
Age, mean (SD)	22.5 (2.5)	21.2 (3.1)	25.0 (4.5)	23.5 (6.4)	36.4 (10.1)	35.2 (10.5)		
Sex (F/M)	13/12	16/13	56/53	31/50	75/70	45/54		
Ethnicity (HC/PT)	Caucasian (12/14) African & other (6/11) Mixed (2/2) Unknown (5/2)		African (43/26) Japanese (36/30) Caucasian (26/19) Other Asian (2/3) Hispanic (0/1) Mixed (1/1) Unknown (1/1)		Japanese			
Education (year)[b]	12.6 (0.9)	11.9 (1.2)*	15.0 (2.2)	13.2 (2.8)**	15.8 (2.3)	13.8 (2.4)**		
Smoking (Y/N)[c]	5/10	16/10	4/79	16/48*	11/78	13/52		

Substance (Y/N)[d]	0/25	4/25	2/107	11/67*	0/145	0/145
DOI (year)				1.2 (0.8)		12.2 (7.7)
CAARMS						
positive [e]		14.3 (6.8)				
total		51.1 (17.1)				
PANSS						
positive [f]				14.6 (4.9)		16.1 (5.2)
negative				16.3 (5.8)		18.1 (6.4)
general				37.3 (11.1)		34.1 (11.1)
CP eq [g]				315.7 (329.4)		451.4 (486.7)
Mean tSNR	1910.4 (387.9)	1956.9 (697.5)	7315.6 (5555.1)	8647.7 (6928.1)	11482.7 (8849.5)	9468.5 (8977.8)

* $p<0.05$
** $p<0.001$
a: No significant difference between HC and PT unless otherwise indicated.

b: Completed years of education were significantly shorter in the UHR ($t=2.4$, $df=51$, $p=0.018$), FEP ($t=5.1$, $df=185$, $p<0.001$), and ChrP ($t=6.5$, $df=238$, $p<0.001$) PTs than in HCs.

c: Information about smoking was available from the IoPPN, JHU, Kyoto, OSK, and Tokyo sites. There were more current smokers in the FEP PT group than in the HC group (Chi-square=12.5, df=1, p=0.001 by Fisher's exact test).

d: Subjects from Japanese sites had no experience of substance use. There were more substance users in the FEP PT group than in the HC group (Chi-square=10.6, df=1, p=0.002 by Fisher's exact test).

e: CAARMS positive scores were available for 26 UHR PT.

f: PANSS positive scores were available for 76 FEP and 94 ChrP PT.

g: One UHR subject was administered 50 mg quetiapine. Medication dose information was available from 55 FEP and 72 ChrP patients.

Abbreviations

CAARMS, comprehensive assessment of at-risk mental states; ChrP, chronic schizophrenia; CP eq, chrolpromazine equivalent; DOI, duration of illness; F, female; FEP, first-episode psychosis; HC, healthy control; UHR, high risk; IoPPN, Institute of Psychiatry, Psychology, and Neuroscience; JHU, Johns Hopkins University Hospital; KMU, Kanazawa Medical University; M, male; N, no; OSK2, scanner number 2 of Osaka University; OSK3, scanner number 3 of Osaka University; PANSS, positive and negative syndrome scale; PT, patients; Tokyo, The University of Tokyo; tSNR, temporal signal/noise ratio; TYM, Toyama University; Unmed, unmedicated; Y, yes.